ABSTRACT

Title of Document:	DEVELOPMENT OF A DIELECTRIC ELECTRO ACTIVE POLYMER ROLL ACTUATOR WITH DIFFERENT BIASING ELEMENTS
	Oscar E. Alvarado, Masters of Science, 2015
Thesis directed By:	Professor Alison Flatau, PhD. Department of Aerospace Engineering

This thesis presents the fabrication and characterization of a tubular Dielectric Electro-Active Polymer (DEAP) actuator system using different biasing mechanisms. DEAPs are attractive in the aerospace community due to their light weight, low electrical power consumption and no noise. A biasing mechanism is needed to supply the DEAP actuator with an optimal pre-load, and its design has a major impact on the overall actuator performance. The biasing elements considered are a conventional linear positive-stiffness bias (PSB) spring, and a constant force bias (CFB) spring. These biasing elements are paired with a roll DEAP actuator and experimentally tested under quasi-static and dynamic loading conditions with a focus on the stroke and blocked force capabilities. The experimental results indicate improvement in stroke using a CFB element but at the cost of blocked force. Work potential is found higher using a PSB than a CFB mechanism.

DEVELOPMENT OF A DIELECTRIC ELECTRO ACTIVE POLYMER ROLL
ACTUATOR WITH DIFFERENT BIASING ELEMENTS

By

Oscar E. Alvarado

Thesis submitted to the Faculty of the Graduate School of the
University of Maryland, College Park, in partial fulfillment
of the requirements for the degree of
Masters of Science
2015

Advisory Committee:
Professor Alison Flatau, Chair/Advisor
Professor Sung Lee
Professor Allen Winkelmann

Dedication

Dedico este trabajo a mis padres Gonzalo y Teresa. Los quiero mucho, gracias por apoyarme en todo. Ustedes me enseñaron que todo se puede en esta vida.

Acknowledgements

I would like to express my deepest gratitude to my advisor Dr. Alison Flatau for her full support, guidance, understanding, and encouragement throughout my study and research. Without her incredible patience and timely wisdom, my thesis work would have been a frustrating and overwhelming journey. I am extremely thankful to her for giving me the opportunity to do such interesting research.

I would also like to thank Dan Clingman for his mentorship throughout the course of my research. This project and thesis would not be possible without him. He has always made himself available to answer any questions I had and lead me to the right path when I felt lost. I also appreciate the time he took to host me during my visit to Boeing in Seattle.

My sincere appreciation is extended to Dr. Lee and Dr. Winkelmann for having served on my committee. Their thoughtful questions and comments were valued greatly.

Special thanks to my colleagues Aaron Sassoon, Ganesh Raghunath, Zohaib Hasnain, Jose Mondragon, and Dr. Suok-Min Na. Their support around the lab was crucial for getting things done. Also, I would like to thank Robert Vocke for his support and guidance using the lathe and milling machines and getting access to the composites lab. Also, I would like to give thanks to Greg Gremillion for his support using the 3D printing equipment.

Table of Contents

List of Tables

List of Illustrations

Chapter 1 Introduction

1.1 Background and Motivation

In aerospace applications, actuators are used everywhere including positioning devices, release mechanisms, aperture opening and closing devices, etc. The need to reduce the size, mass and power of these actuators is of increased interest and a lot of research has been put on finding new transducer technologies. From those efforts, the Dielectric Electro Active Polymer (DEAP) or Dielectric Elastomer (DE) technology has gained considerable attention due to its high energy, high efficiency, fast response and silent operation [1].

As seen in figure 1.1, DEAPs cover the medium force density and strain region where other dominant actuator technologies do not. This opens the possibility to improve or develop new devices. Some prototype devices using DEAP materials have been built including valves [2, 3], robots [4, 5], pumps [6], active hinges [7] and loudspeakers [8]. However, even with the popularity of DEAP in the research community, the amount of DEAP devices in industry is very low mainly because of the lack of knowledge needed for building such device.
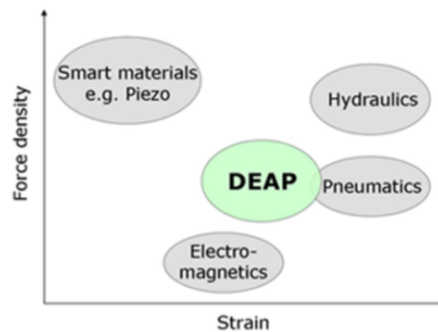
Figure 1.1 DEAP technology performance capabilities in terms of relative force density and strain capability compared to other dominant actuator technology capabilities [9]

As new DEAP materials emerge, challenges arise associated with understanding the material behavior and the design of a device that uses the new material. The general objective of this thesis research is to characterize the behavior of a new commercially available DEAP material and develop an actuator based on this material. This actuator could potentially work as a pump, valve or micro positioner.

1.1.1 Electro Active Polymers (EAP)

Dielectric Elastomers (DEs) or Dielectric Electro Active Polymers (DEAPs) belong to a broader group of smart materials known as Electro Active Polymers (EAPs). EAPs are polymers that exhibit a change in size when stimulated by an electric field and can be divided into two principal classes: Ionic EAP (actuation caused by the diffusion of ions) and Electronic EAP (actuation driven by electric field or Maxwell stresses) [10]. Current available leading EAP materials are listed in table 1.1 and a summary of advantages and disadvantages of these two groups are listed in table 1.2.

In this research, a Dielectric Electro Active Polymer material is used to developed actuators and as seen in table 1.1, it belongs in the electronic subgroup

Table 1.1: List of leading EAP materials [10]

Electronic	Ionic
Electrostrictives	Ionic Polymer Gels
Ferroelectric Polymers	Carbon Nanotubes
Dielectric Electro Active Polymers	Conductive Polymer
Liquid Crystal Elastomers	ElectroRheological Fluids

Table 1.2 Summary of advantages and disadvantages of the two EAP material classes [10]

EAP type	Advantage	Disadvantage
Ionic	• Low activation voltage (2-10 V) • Bi-directional actuation that depends on voltage polarity	• Requires electrolyte • Electrolysis occurs in aqueous systems at >1.23 V • Requires enclose to operate in open air conditions • Slow response (fraction of a second) • Most materials do not hold a strain under DC voltage
Electronic	• High mechanical energy density • Can hold strain under DC voltage • Rapid response (mSec) • Low power consumption (mW)	• Requires high activation voltages (2-10kV) • Produces monopolar actuation (polarity independent)

1.1.2 History of DEAP Technology

The transduction mechanism behind DEAPs has been observed and understood for many years; long before this category of smart materials was introduced and began to use DEAP attributes to advantage. The study behind the repulsion and attraction forces of charged particles, known as Coulomb's law, dates back to the 1700's when French physicist Charles Augustin de Coulomb published his first three reports on electricity and magnetism. However, the field of DEAP smart materials was not established until 1986 when a theoretical study of the Maxwell stresses on dielectric materials was performed by Anderson [11]. His work was then followed by Zhenyi et al. in 1994, who conducted experiments using polyurethane films between Tin foil electrodes and were able to produce 3% strain in the thickness direction [12]. At the time, this was a great accomplishment since piezoelectric materials, the only other electrically actuated

materials, were producing only a fraction of a percent strain. In addition, Zhenyi et al.'s work shed light on the importance of compliant electrodes after noting how the rigid Tin foils electrodes may have had a negative impact on the response of the polymer. Zhenyi's work and similar studies performed in the following years gave rise to the realization of the DEAP technology.

Early work on DEAPs mainly came from Pelrine and others from SRI International. Initially they were able to produce in-plane strains of up to 10%-32% using silicone as a dielectric material [13]. This number was later surpassed by the introduction of acrylic as a dielectric material. In 2000, they published a paper using acrylic VHB 4910 that produced strains that easily broke the 100% strain mark [14]. Their contributions also include the use of roll DEAP linear actuators to drive a prototype 6-legged robot capable of moving at 3.5cm/s [15], out of plane actuators [16] and the application of DEAPs as loudspeakers [8]. Other significant contributions came from Carpi who conducted experimental and theoretical research on DEAPs. He studied the use of different electrodes [17], developed a model for cylindrical actuators and fabricated helical and folded actuators [18, 19, 20].

1.2 DEAP Operating Principle

DEAP materials are essentially compliant capacitors where the dielectric material is a soft elastomer film that is sandwiched between two compliant electrodes. When a high electric field is applied, the coulomb forces cause an attraction between the electrodes which squeeze the elastomer dielectric material resulting in a decrease in thickness and expansion in planar directions (see figured 1.2). Typical activation voltages range from 2-10kV, but the consumed current is very low therefore having low power consumption as listed in table 1.2.

electrodes
elastomer

Lo
to
Wo
Voltage off

Lo + ΔL
to-Δt
Wo + ΔW
Voltage on

+
–
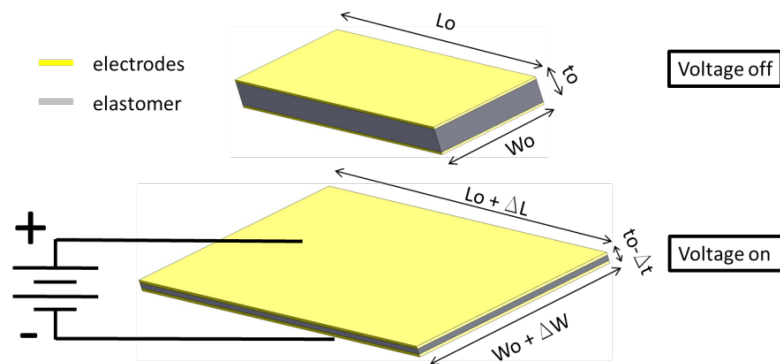
Figure 1.2 DEAP material working principle showing volume conservation as voltage is applied causing a decrease in thickness and an increase in planar surfaces area.

1.2.1 Danfoss Polypower DEAP Material

One of the strengths of the DEAP technology is the ability to use a wide range of materials as the elastomeric dielectric layer. Polymers as soft as gels and rigid thermoplastics can be used as the dielectric layer. However, silicones and acrylics are the popular materials of choice since they are known to have high electrical breakdown strength, low modulus, high permittivity and good elastic properties [1].

The material used in this work is commercially available from Danfoss Polypower A/S and was obtained as part of their evaluation kit. It is a silicone based DEAP material that has a special corrugated surface and a very thin layer of silver electrodes on top of it. The corrugation pattern in the dielectric layer makes the DEAP film compliant in one planar direction and stiff in the orthogonal direction (see figure 1.3). The principle of operation is the same as in any other DEAP material. However, the ability to deform in preferentially one direction ensures better uniaxial actuation performance than in alternative designs where the material simultaneously elongates in two directions [9]. This innovative material will be used in the actuators presented in this thesis and its characteristics are shown in table 1.3.
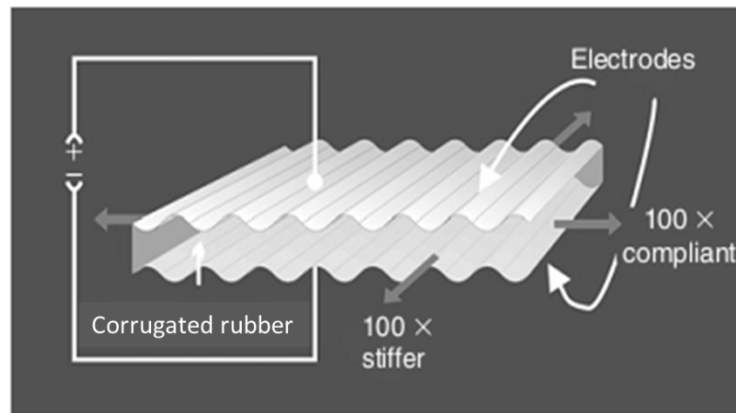
Figure 1.3 Danfoss Polypower DEAP material technology illustrating the corrugated pattern used for creating compliance and stiffness in orthogonal planar directions [9]

Table 1.3 Danfoss Polypower DEAP Material characteristics [9].

Danfoss Polypower Material Characteristics			
Strain limitation in compliant direction	Strain limitation in stiff direction	Maximum activation Voltage	Film thickness
30 %	1 %	2500 V	80μm
Elastomer material properties			
Relative Permittivity	Young's Modulus		Density
3.1	1.1 MPa		1.11 g/cm^3

1.3 Importance of Pre-Strain

As previously discussed, excellent material performance found in DEAP materials can be attributed to different factors including the discovery of new materials and improvements in electrode technology such as the corrugated material used in this research. However, much of the improvement in material performance is due to pre-strain [21]. Pre-strain is defined as the initial strain loading condition that is produced by stretching and holding the DEAP film in tension before voltage is applied. Previous research has shown that introducing a pre-strain in the DEAP material can significantly increase the maximum amount of actuation strain and pressure generated within a given film. For example, work by Pelrine, Kornbluh, Pei and Joseph on biaxially and uniaxially pre-strained films resulted in actuated strains up to 117% with silicone elastomers and 215% with acrylic elastomers [14]. These strains surpassed those actuator strains without pre-strain. Other studies [22, 23] revealed that supplying a pre-strain on the material increases the its breakdown strength in some cases as much as 10 times that obtained with no pre-strain.

The reason why pre-strain enhances material performance can be explained by Pelrine's equation (see equation 1.1). His equation has been accepted and validated for use in accurately representing the electromechanical coupling in DEAP actuators [24, 25]. It essentially describes the relationship between the mechanical pressure (P), generated across the sample thickness, i.e. normal to the planar surface area of the film, and the voltage (V) applied across the sample's two electrodes.

$$P = \varepsilon_o \varepsilon_r \left(\frac{V}{t}\right)^2 \qquad\qquad 1.1$$

The equation indicates that the thickness (t) of the DEAP material is inversely proportional to the amount of pressure generated by the electrostatic forces. In other words, decreasing the thickness of the material increases the transduction of electrical energy to mechanical energy.

A number of different pre-strain mechanisms have been used in DEAP devices. For example, in cone-shaped DEAP actuators, the film is attached to a frame and pre-strained out of plane by an internal spring as seen in figure 1.4 [26]. Another study investigated using internal pressure and coil springs in pre-straining tubular actuators [27, 28].
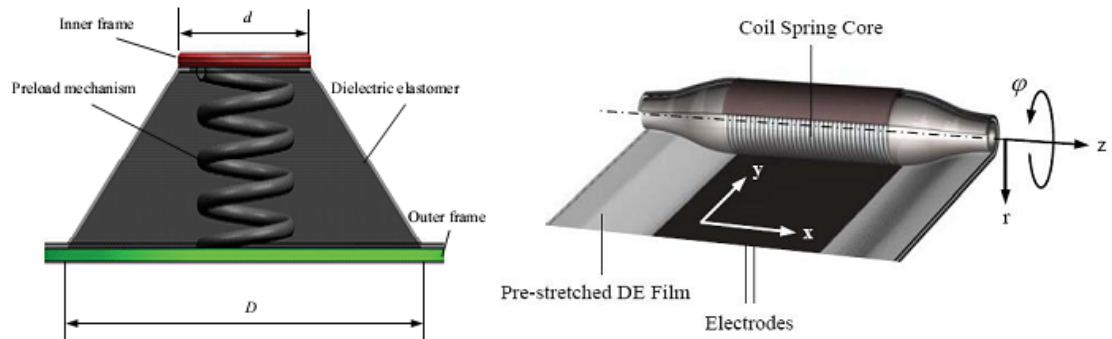
Figure 1.4 Cone DEAP actuator pre-strained out of plane by coil spring (left). Tubular actuator with coil spring pre-strain mechanism(right) [26, 27].

As it will be shown in a later chapter, the type of pre-strain mechanism has a pronounced effect on the performance of the actuator. Therefore, designing a mechanism to pre-strain the DEAP film is one of the goals of this project. The actuator pre-strain and biasing fundamentals will be explained in more detail in Chapter 3.

1.4 Actuator Configurations

The working principle of a DEAP film is fairly easy to understand, but it does not really explain how to make a practical actuator. The film not only needs to change shape but also be able to move something. Because of its simple structure, DEAPs can be configured into many practical actuators. Some of the basic configurations are shown in figure 1.5 where the arrows show the direction of actuation and the light and shaded regions represent the elastomer film and electrodes.
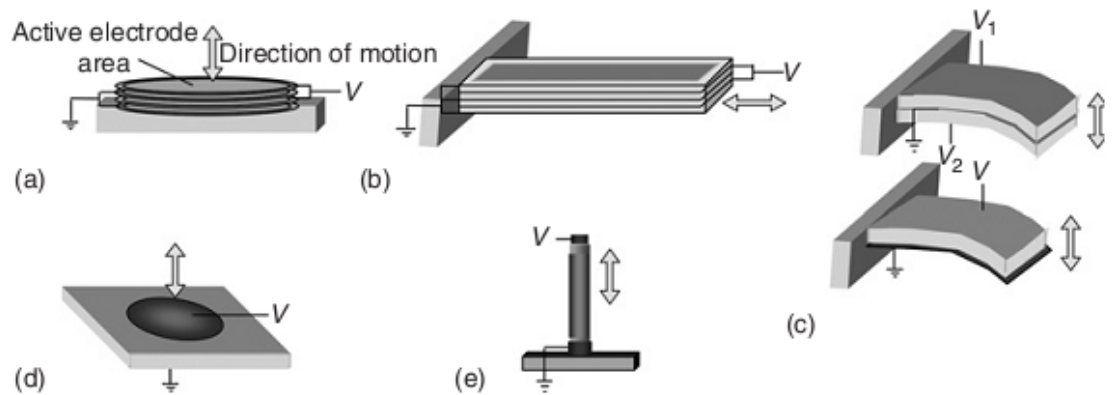
Figure 1.5 Basic DEAP actuator configurations with a bidirectional arrow depicting the directions of output motion: a) stack, b) extender, c) bimorph and unimorph bending beam actuators, d) diaphragm and e) tube or roll [29]

The roll or tubular configuration is studied in this research. The main advantage of this configuration, as with a stack configuration, is that it can use a large volume of

DEAP material in a compact package. In other words, the configuration enables large active cross-sectional areas and therefore high actuation forces.

1.4.1 Tubular or Roll Actuators

The tubular or roll actuator is popular in the DEAP research community. Carpi et al. and De Rossi et al. conducted studies on single layer cylindrical DEAP actuators. They measured axial strains of 4.5% with a 5% axial pre-strain and developed an electromechanical model [30]. Zhang et al. developed miniature rolled DEAP actuators used in a portable force feedback device [27]. These actuators were manufactured in a machine-aided process and consisted of a stack of two biaxially pre-stretched acrylic DEAP films wrapped around a fully compressed coil spring (see figure 1.6). The actuator is known as the "spring roll" and a similar version will be developed in this research.
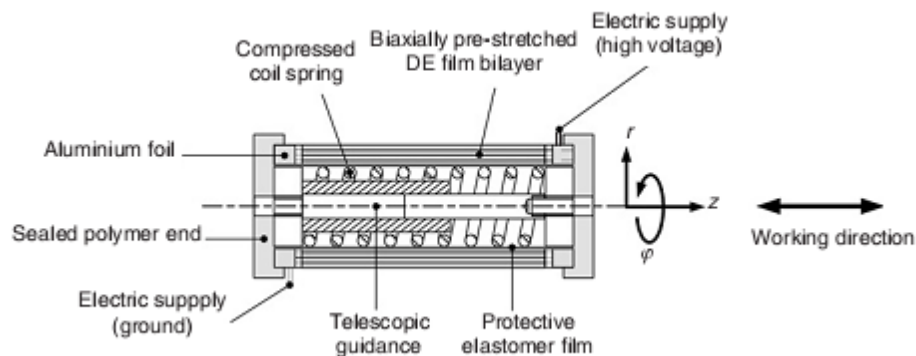
Figure 1.6 Spring roll actuator schematic. A compressed spring is used to pre-strain DEAP film in the axial direction and circumferential direction while a telescopic guide is used to insure the actuator moves in the working direction. [27]

Danfoss Polypower A/S also developed roll actuators using their unidirectional DEAP material (see figure 1.7). These push actuators do not contain any pre-strain mechanism and have a large cross-sectional in order to be self-supported. Data presented show 1.7% peak strain and 13KPa peak actuation pressure [31].

Figure 1.7 Danfoss Polypower "inlastor" push actuators [31]. The actuators contain no pre-strain and are self-supported due to their large cross-sectional area.

1.5 Thesis Overview

This thesis presents the development and characterization of roll actuators using the unidirectional DEAP material with corrugated surface. Chapter 2 explores the design and fabrication behind the simple roll actuator using the Danfoss Polypower material. Chapter 3 presents a study on the effect of pre-strain in the DEAP output displacement and force. In chapter 4, the development and characterization of a spring roll actuator will be discussed. Chapter 5 will present a second actuator with a constant force pre-strain mechanism. Finally, Chapter 6 provides a summary of the conclusions that can be drawn from the results of these different studies.

Chapter 2 Actuator Fabrication

This chapter describes the fabrication of a roll or tubular spring actuator using the Danfoss PolyPower A/S DEAP material. A computer-aided representation of the steps is presented leading the actual manufacturing steps.

2.1 Configuring DEAP Film into a Useable Element

When it comes to building an actuator, the basic form of the DEAP film is not very practical. The electrical leads need to be placed where the material is not active to avoid failure of the electrodes due to fatigue. Additionally, the passive area is useful for minimizing potential for shorting of the electrodes and for providing a mounting surface for the boundaries of the actuator. As a result, part of the electrode coating is removed with an etching process as seen in figure 2.1. The active region represents the area of the film where the electrodes overlap and expand under electrical stimulus. The passive regions do not experience deformation and are used as the mounting surface and to attach electrical leads.
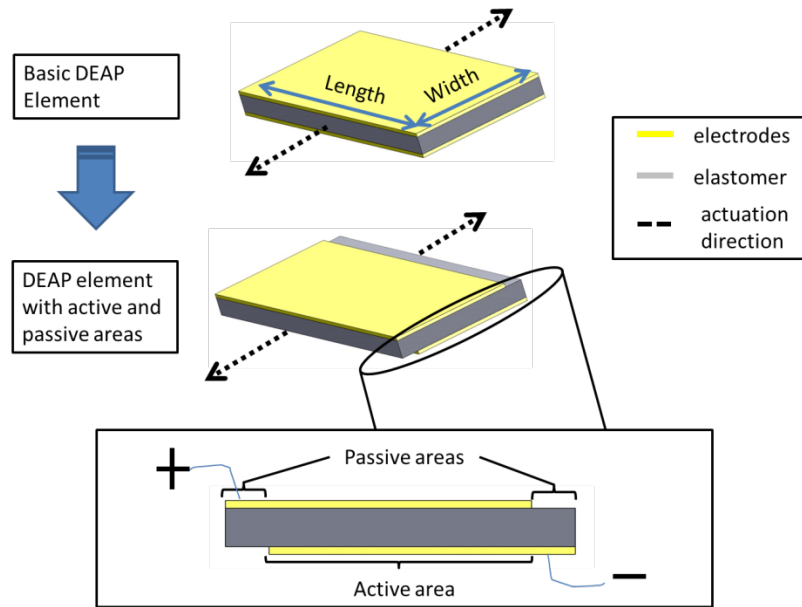
Figure 2.1 CAD representation of the DEAP film in its basic form (upper) and with electrodes removed (lower). The lower image shows regions of the upper and lower electrodes that are made passive by etching away the electrode.

An additional band of electrodes is also removed along the width of the film to prevent electrical arcing at the edges (see figure 2.2). In this case, the electrodes are removed from both top and bottom of the film hence leaving only the elastomer at the edges of the active region.

It is important to note that all of these regions where the electrode is removed damp out the deformation of the DEAP material. Some studies have looked at these effects and concluded that reduction of the width of the passive regions incrementally increase achieved performance [31]. Hence, the width of the passive regions normal to the actuation direction is set to 5 mm and the passive regions long the active direction is set to 2mm (see figure 2.2).

The final state of the DEAP film is shown in figure 2.2. The views of the top and bottom sides of the film depict two very important design parameters in a DEAP actuator: the active width (w_a) and active length (L_a). They represent the dimensions of the area of the overlapping electrodes and will be used frequently throughout the rest of this research.
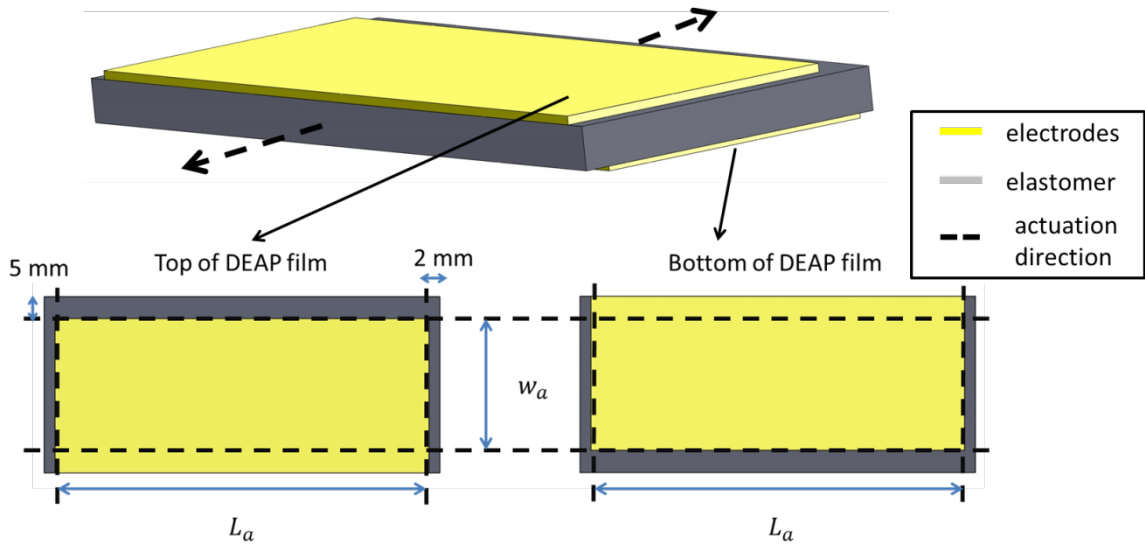
Figure 2.2 Final state of DEAP sheet as prepared for use in an actuator. A 5mm-wide band of electrode has been etched-away from the edges normal to the actuation direction on the upper and lower surfaces. Another 2mm wide band of electrode has been etched-away from the edges parallel to the actuation direction.

2.2 Roll or Tubular Configuration

At this point, the DEAP film is ready to be configured into a roll or tubular actuator. For the sake of clarity, the top and bottom electrodes of the film will now be represented by different colors and the electrodes removed along the active width will not be shown in the figures.

The tubular or roll design simply consists of winding the DEAP film in a cylindrical manner. One of the first challenges encountered deal with shorting the DEAP film upon rolling. If configured into a cylinder as shown in figure 2.3, the surface of the bottom electrode faces the surface of the top electrode leading to an electrical short.
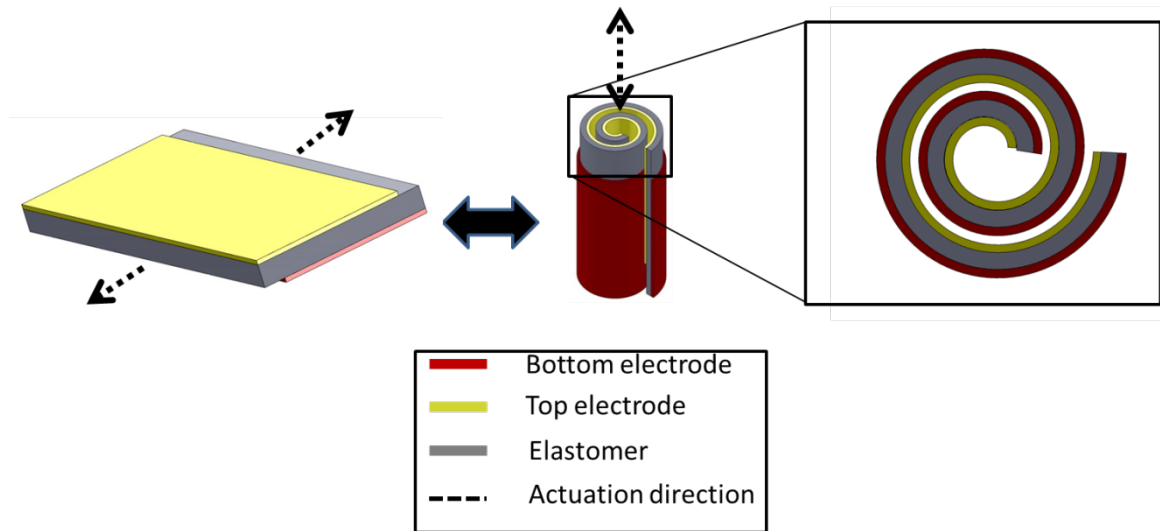
Figure 2.3 Schematic of DEAP element in its planar (left) and roll configuration (right). The cross-sectional view of the roll configuration shows the induced electrical short when a single DEAP sheet is used.

To overcome that problem, two DEAP sheets are adhered together along passive areas and electrically connected as seen in figure 2.4. This composite configuration has the same surface area for active and passive regions but now when wound into a cylinder, the electrode polarity is isolated from one another, so that shorting does not occur.
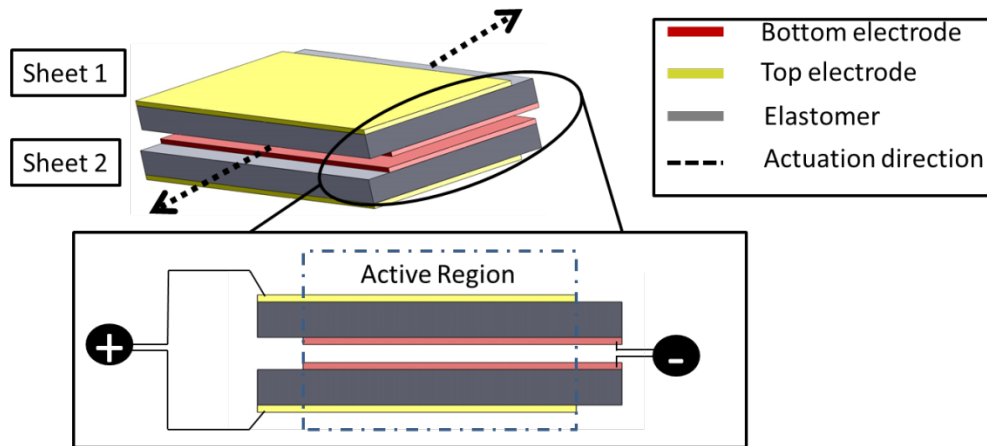
Figure 2.4 DEAP composite configuration. Two DEAP sheets are bonded along the passive regions normal to the actuation direction. The inner electrodes are connected and the same goes for the outer electrodes.

The composite configuration is the foundation behind the roll actuator design and it was used in the actuators built in this project. In the next section, the manufacturing steps and tools to get to the composite configuration are discussed.

2.3 DEAP Material Handling and Composite Configuration

A lot of time was spent learning how to handle the Danfoss Polypower DEAP. The fragility of the electrodes and the material's high elasticity made handling of the material difficult. Multiple iterations were needed before reaching a good fabrication procedure and only the relevant ones are presented here.

The important aspects of the composite configuration are the electrode removal and adhesion of the two sheets. Part of the challenge is that the passive and active areas created in the two sheets need to be as identical as possible.

Initial methods consisted in gluing the material ends to a clean surface and using a paper or plastic guide to trace the active-passive markings onto the material. While this marking method worked, manually gluing the two sheets accurately was difficult.

An improved method was conceptualized with the help of 3D printed tools (see figure 2.5). Here, the tools were modeled in SolidWorks and sent to an Object 3D printer. The fabrication table is used to hold the DEAP material in place while the passive and active areas are created by the respective markers shown in figure 2.6
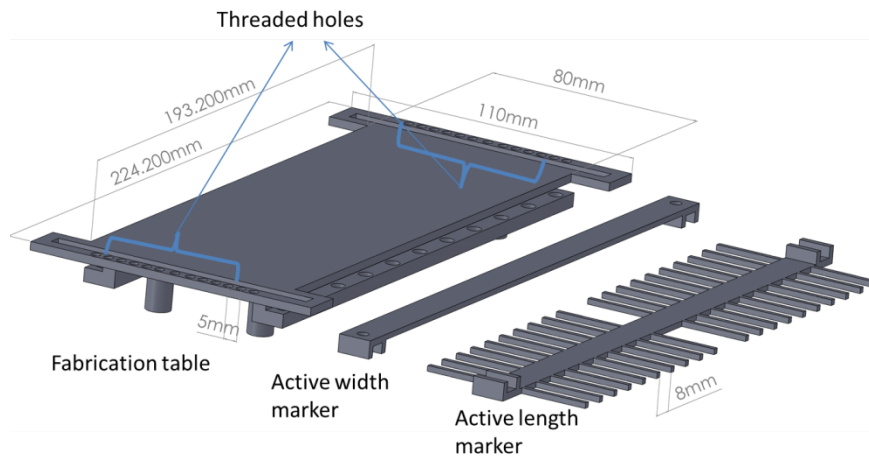
Figure 2.5 CAD views of 3D printed tools used to create DEAP composite configuration. The fabrication table has threaded holes to hold the marking tools. The dimensions of the tools are based on the size of the built actuators in this thesis.

The tools served three purposes:

- Decrease operator handling

- Accurate removal of electrodes (creation of active and passive areas)

- Accurate adhesion of the DEAP sheets

Figure 2.6 shows a general summary of the manufacturing steps using the 3D printed tools. The film is cut using a razor blade and the electrodes removed using swabs

and Clorox cleaning product containing 5% chlorine. The glue used is a silicone adhesive named Elastosil E43 from Wacker silicones and the electrical leads are made from thin copper tape. Step five is the composite DEAP structure ready to be configured into a roll actuator. The tools and steps shown in figure 2.5 and 2.6 are used for the actuators presented in this research.

1) Material is mounted on fabrication table at the edges
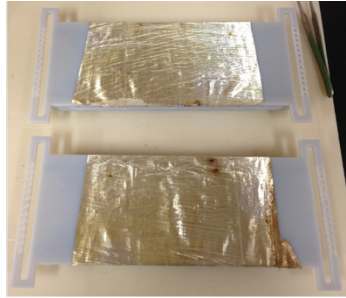
2) Marking of passive and active areas
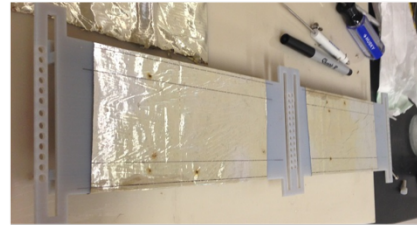
3) Electrodes removed. Active and passive areas created

w_a

L_a
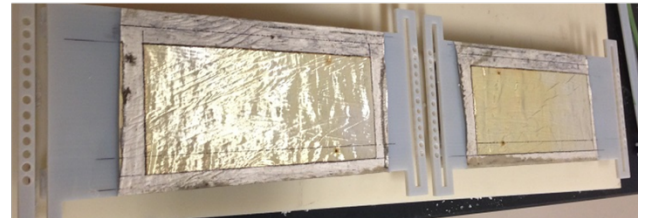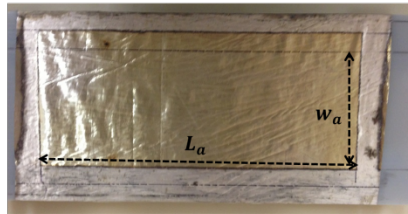
4) Sheets glued together. Electrical lead placed for inside electrodes (not visible)
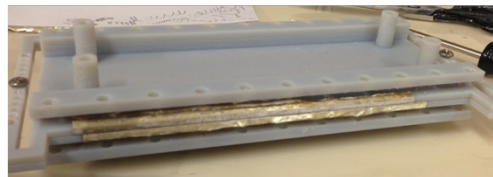
5) Composite configuration
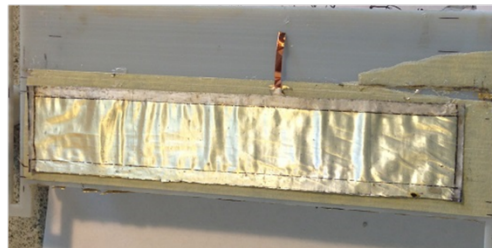
Figure 2.6 General summary of DEAP composite fabrication steps 1-5 with descriptions indicated at the left.

To obtain the roll configuration, round plastic mounts were built. Initially, a lot of time was spent machining plastic into a desirable mount but the use of 3D printers expedited the design and building efforts. Figure 2.7 shows the CAD model of the mounts used in one of the actuators.
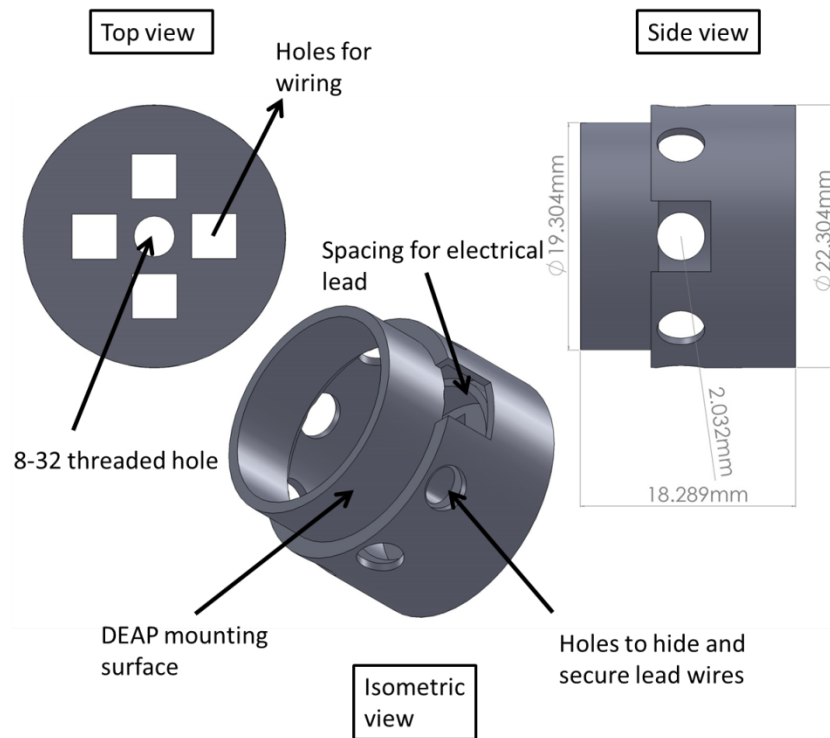
Figure 2.7 Different CAD views of a typical end mount with descriptions and dimensions of its main features.

The mounts are designed hollow to reduce the overall mass of the actuator but their main purpose is to provide an attachment interface to other surfaces. For some of the actuators presented in this research, the mounts will have different features but the same characteristics shown in figure 2.7.

A metal stand was assembled to help wind and attach the DEAP film to the mounts (see figure 2.8). After the winding is complete, the actuator is left overnight to let the silicone glue cure. The high voltage wires are then soldered to the copper leads and finally, the actuator is removed from the metal stand.
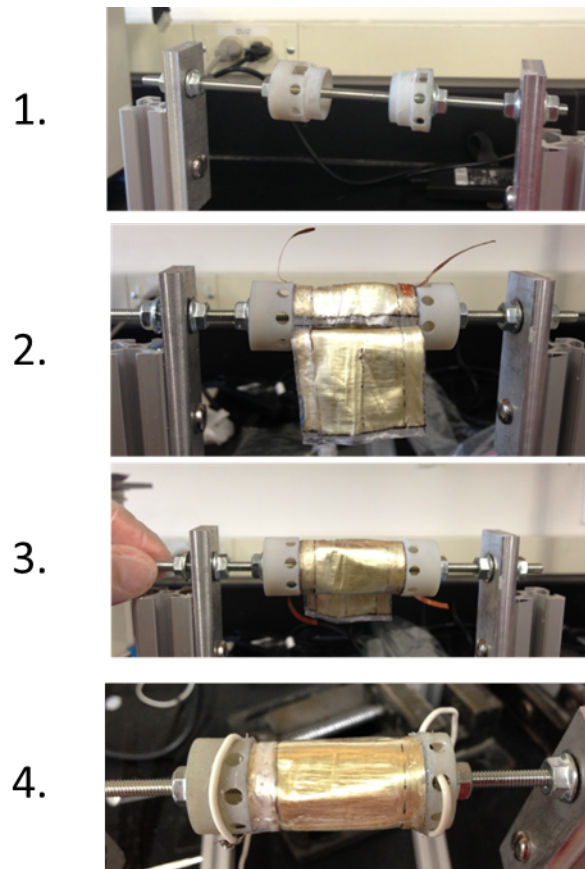
Figure 2.8 Example of winding procedure. The mounts are spaced apart at a distance dictated by the actuator (1). Material winding and bonding process (2-3). After winding is complete, the silicone glue is left to cure overnight. High voltage wires are then soldered to actuator leads and are secured within the mount end (4)

2.4 Summary

In this chapter, the fabrication of a basic roll actuator was presented. With the help of 3D printed tools, the manufacturing of these devices were possible. Electrode removal and gluing of the two DEAP sheets together were found as the key parts in the fabrication process. The manufacturing presented here will be used on the three actuators built and characterized in chapter 3, 4 and 5.

Chapter 3 DEAP Material Pre-strain Characterization

This chapter conducts qualitative analysis of the effect of pre-strain on the performance of the DEAP material used in this research. As explained in chapter 1, pre-strain is the initial loading condition before voltage is applied to the material. The tests presented in this chapter will determine the optimal pre-strain level that will be applied to the DEAP actuators.

3.1 Pre-strain Principles

In this research pre-strain will be defined by the symbol l. Its mathematical representation is shown below (equation 2.1).

$$l = \left({}^{\Delta L}/_{W_a}\right) * 100 \qquad\qquad 2.1$$
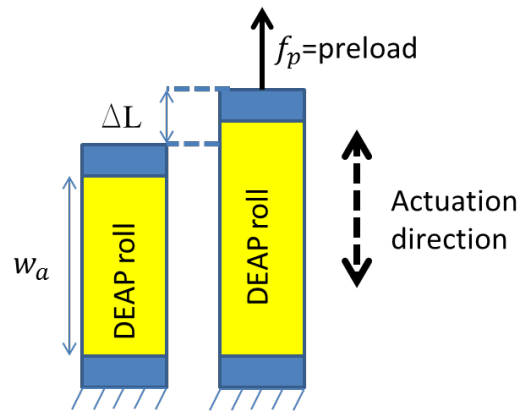
Figure 3.1 Schematic of pre-strain principle on DEAP actuator. Pre-strain is applied in the direction of actuation.

ΔL represents the pre-stretch of the DEAP material in the actuation direction and W_a is the active width of the DEAP sheets used to build the roll (see figure 2.2). A sample DEAP roll is built using the manufacturing steps shown in chapter 2. The built actuator is

show in figure 2.2 and its parameters listed in table 3.1. The active cross-sectional area is given by L_a, the length of active area, and t, the thickness of the DEAP material.

Table 3.1: Properties of DEAP actuator used for pre-strain study

Active geometric properties			Overall Geometry	
Active length (L_a)	Active Width (W$_a$)	Active Cross Sectional area ($A = L_a * t * 2$)	Diameter (D)	Length (L)
95 mm	25.5 mm	15.2 mm^2	22 mm	49 mm
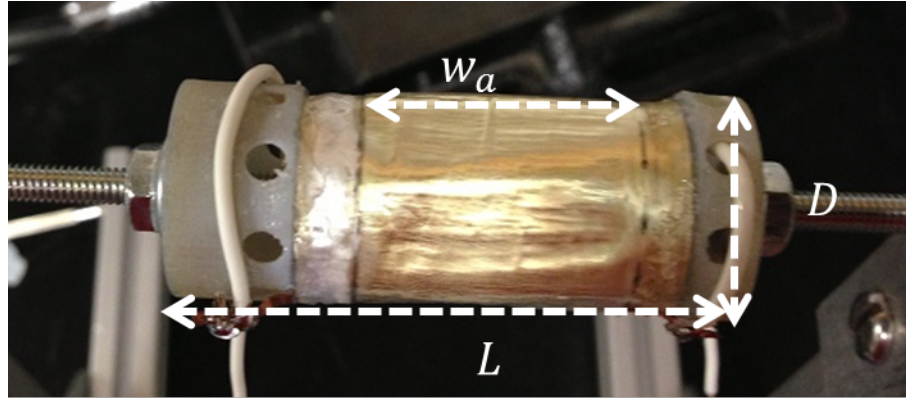
Figure 3.2 Photo of DEAP actuator used in the pre-strain study with its main dimensions labeled.

3.2 Experimental Procedure of Pre-strain Study

A semi-automated experimental procedure was conceptualized. The application of pre-strain is done manually but a Labview code was developed to automatically perform data collection and provide voltage to the DEAP specimen.

The exact experimental procedure is shown in figure 3.2. The Labview code takes over after the pre-strain is applied. The timers are used to wait for the DEAP material to stop creeping. Creep is a viscoelastic phenomenon where the strain of a material

increases with time if held by a constant stress. The film is known to be viscoelastic especially at larger strains hence it is taken into account in the Labview code. Every time the material is pre-strained, a timer is set on to delay the application of voltage as shown in figure 3.2. Another timer is also set on when the DC voltage is applied to the material to delay the data collection. All delay times were chosen based on creep tests on the material.
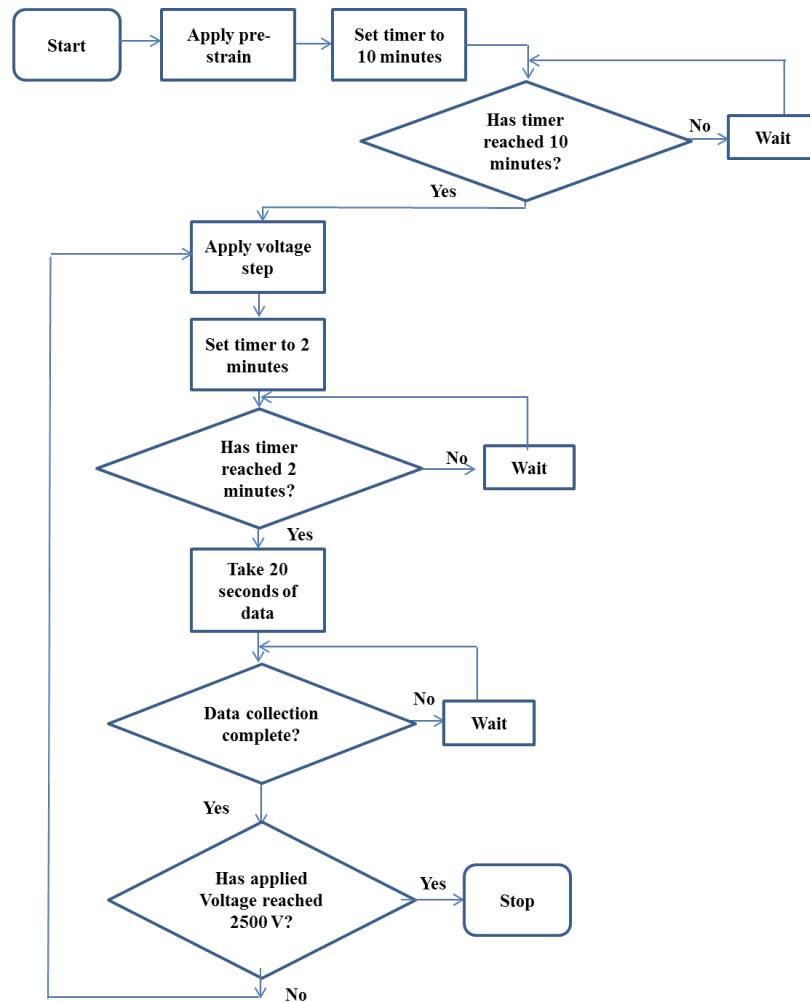
Figure 3.3 Flowchart of pre-strain experimental procedure. A labview code runs the experiment after the pre-strain application step is complete.

3.3 Pre-strain vs. Actuator's Blocked Force

During this experiment, blocked force produced in Actuator 1 is measured for DC voltages applied from 0 to 2500 Volts at a specified pre-strain l. The experimental setup is shown in figure 3.3. The actuator is mounted on a rigid stand with one end connected to a load cell (Honeywell model 31) and the other to the sledge of a home-made translation stage. The load cell measures the pre-load in the DEAP roll and also the blocking force when the actuator is activated. Pre-strain is applied when the orange knob on the translation stage is turned clockwise causing the sledge to move up. The sledge displacement or ΔL is tracked by a MICROTEK II laser displacement sensor.
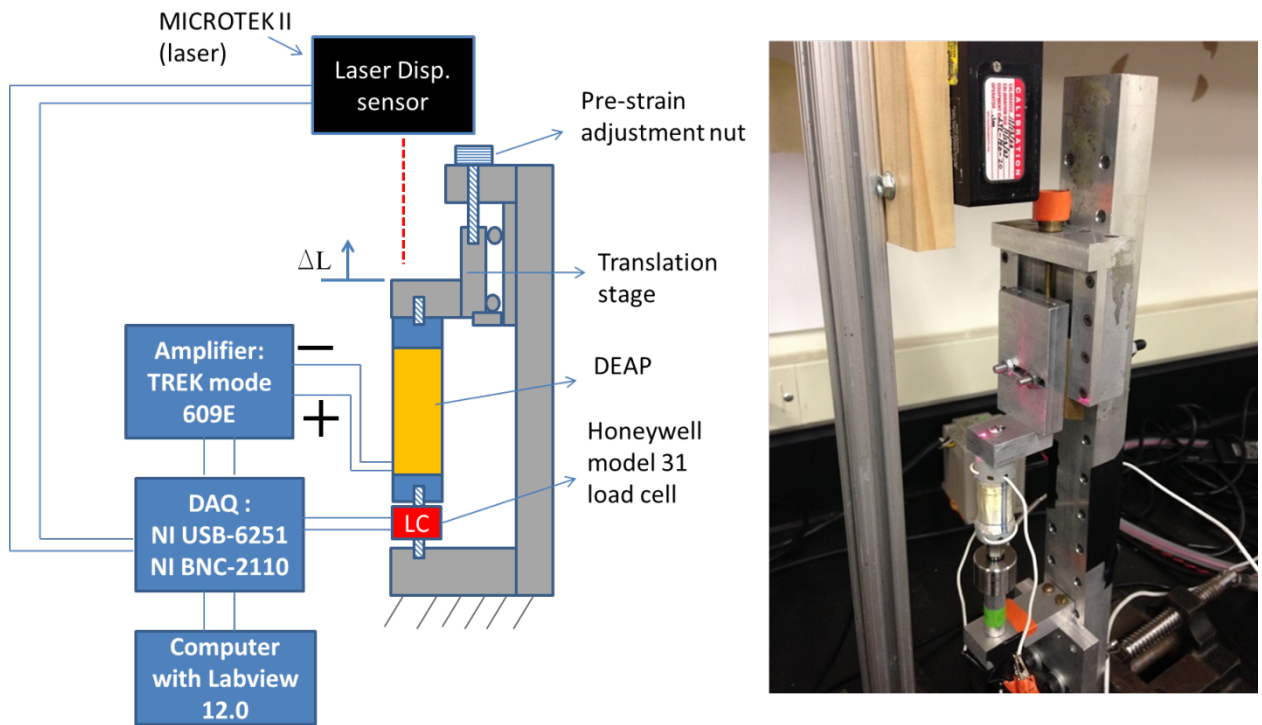
Figure 3.4: Schematic (left) and photo (right) of the experimental setup of pre-strain experiment.

The voltage supplied to the DEAP comes from a TREK high voltage amplifier (model 609E). All signals are processed through a National Instruments USB 6251 DAQ programmed from a Windows laptop computer running Labview 12.0.

3.3.1 Experimental Results

The actuator response at different λ values is shown in figure 3.5. The plot shows the blocked force response for λ values ranging from 0 to 15.3%. It is clear from the figure that an increase in pre-strain results in an increase in blocked force. However this increase is not substantial for all λ values. Once pre-strain is higher than 5%, the effect of pre-strain is small especially at low voltages. Also, the curves get closer together as pre-strain increases suggesting the blocked force is approaching a final value and will no longer increase with pre-strain. Figure 3.6 shows the experimental results in terms of stress.
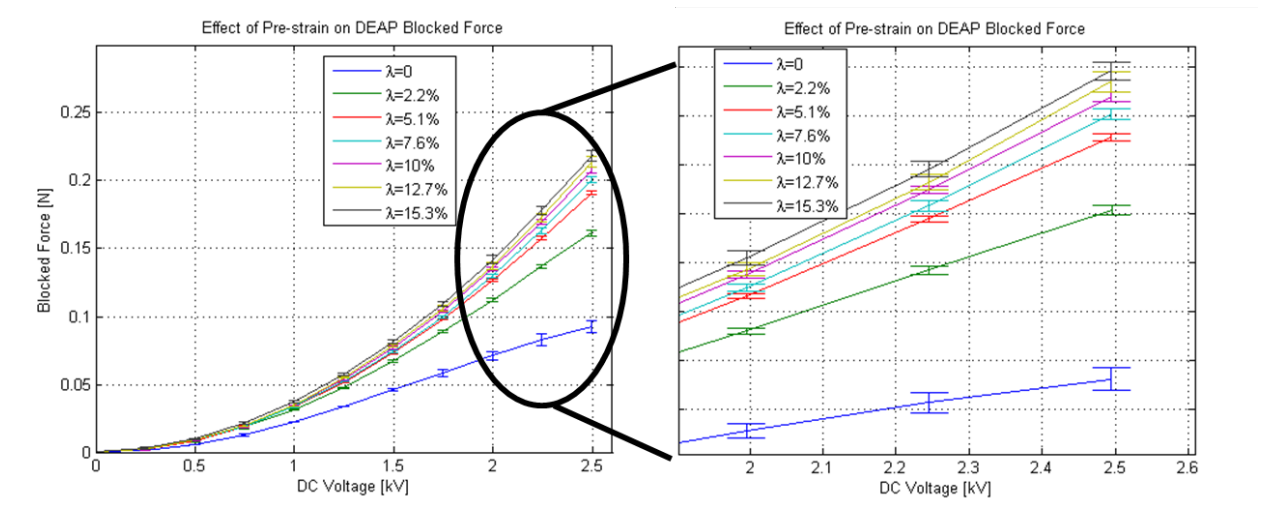
Figure 3.5 Experimental results showing the blocked force (N) response as a function voltage (kV) for different pre-strain values (left). Close up view at higher voltages (right)
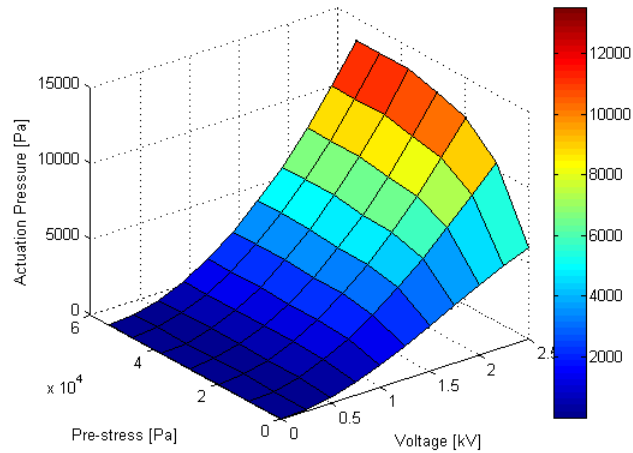
Figure 3.6 Experimental results in terms of pre-stress (Pa), voltage (kV) and actuation pressure (Pa). Pre-stress is the given by the pre-load divided by the active area given in table 3.1. In a similar way, actuation pressure is given by the blocked force divided by the active area.

3.4 Pre-Strain vs. Actuator Displacement:

During this experiment, Actuator 1 is held at a specified pre-strain (1) by a bias spring and its free displacement is measured for DC voltages ranging from 0 to 2500V.

The test setup used in this experiment is very similar to the setup previously used (see figure 3.4). The difference is the pre-strain is now supplied by a linear spring and the actuator is allowed to move (see figure 3.7). Due to size constraints, a rectangular plastic piece was attached to the free end of the actuator in order for the laser beam to track its movement.
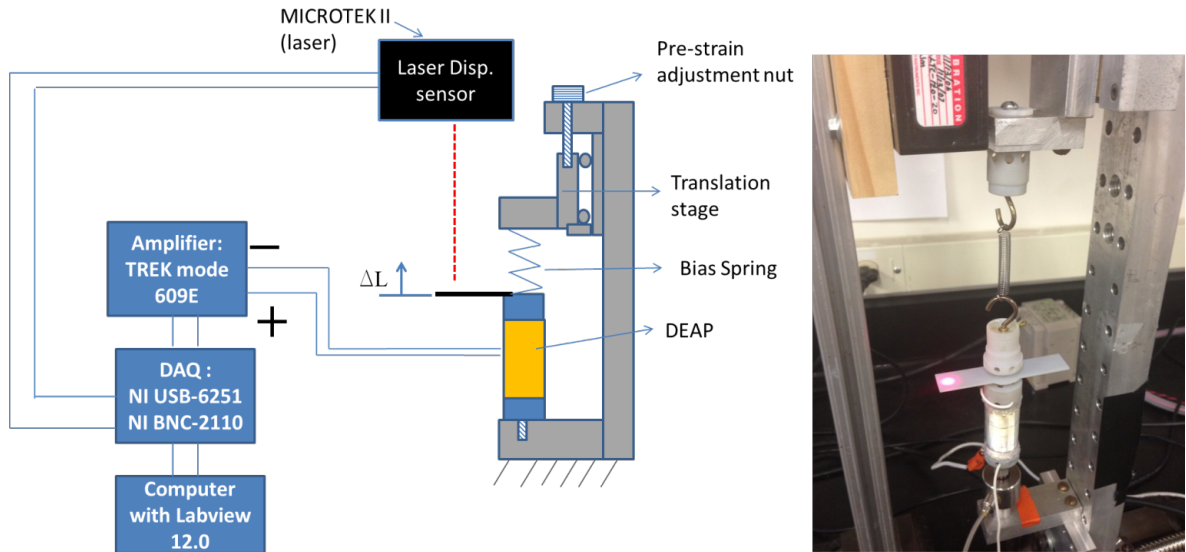
Figure 3.7 Experimental setup used to measure the displacement of Actuator 1 at different pre-strain levels. A bias spring attached to the actuator at one end and to the translation stage at the other supplies the specified pre-strain. A laser tracks the displacement of a rectangular plastic plate attached to actuator free end.

The stiffness of the bias spring was chosen based on the stiffness of the roll DEAP Actuator 1. The tensile load – axial displacement behavior of the actuator was obtained using the setup in figure and is shown in figure 3.8.
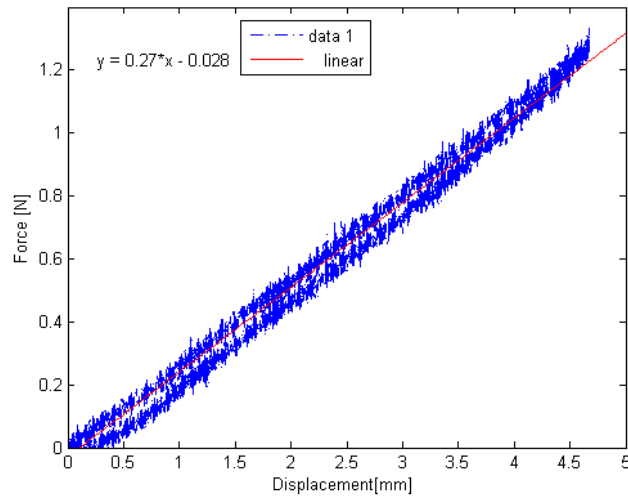
Figure 3.8 Tensile test of DEAP roll in pre-strain study. The tensile load (N) and axial displacement (mm) are measured simultaneously. A linear fit is applied to the data (red line) where the slope of the fitted line indicates the stiffness of the DEAP.

A linear fit of the data is shown by the red line and its corresponding equation. This test is considered an approximation because the loading rate was not controlled and the material is known to be rate dependent. Nevertheless, the slope of the fitted line to the tensile test indicates the actuator has a stiffness of 270 N/m. The bias spring was then chosen a lower value (~50 N/m) to insure the actuator can move relative to the spring.

3.4.1 Experimental Results

Figure 3.7 shows that the effect of pre-strain on actuator displacement for `l` values ranging from 2.5% to 12.3%. As shown, the effect of `l` is minimal overall for the range of pre-strains studied. Especially at low voltages, the effect of pre-strain seems to be negative if not equal. At high voltages however, the effect is more apparent.
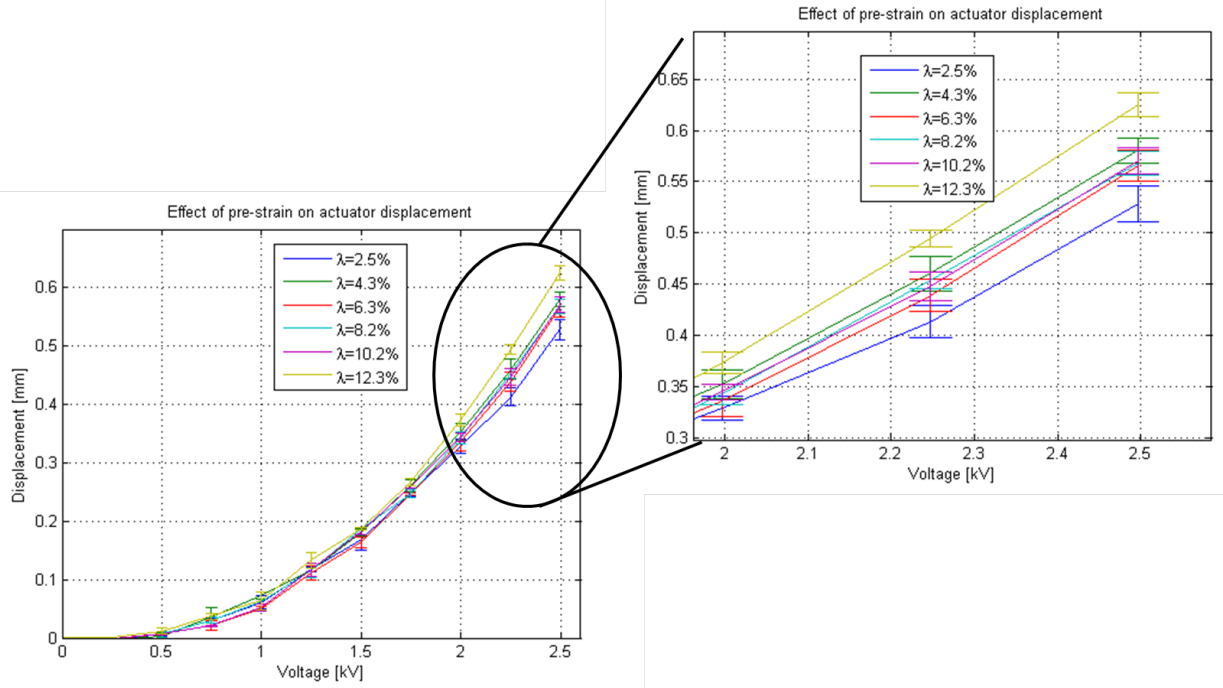
Figure 3.9 Actuator 1 displacement (mm) as a function of voltage (kV) at l values that range from 2.5% to 12.3%

3.5 Effect of pre-load on Displacement

Up to this point, all of the tests have been in terms of pre-strain. However, the type pre-load has a pronounced effect on the actuator output displacement.

Taking a closer look at section 3.4, when the DEAP actuator is pre-strained or pre-loaded, the bias spring and DEAP must be in force equilibrium. If the actuator is then activated, the bias spring and DEAP are in a new force equilibrium.

The force source of the pre-strain (l) or pre-load (f_p) element is essentially from an elastic element or spring and can be categorized into three types depending on its derivative with respect to deformation "y". The three types are the following:

- Positive stiffness $(df_p/dy) > 0$

- Constant force $(df_p/dy) = 0$

- Negative stiffness $(df_p/dy) < 0$.

Figure 3.9 shows the behavior of the pre-load elements and how it matches the DEAP material. The force-displacement curves of the DEAP are approximated to be linear in order to simplify the analysis.
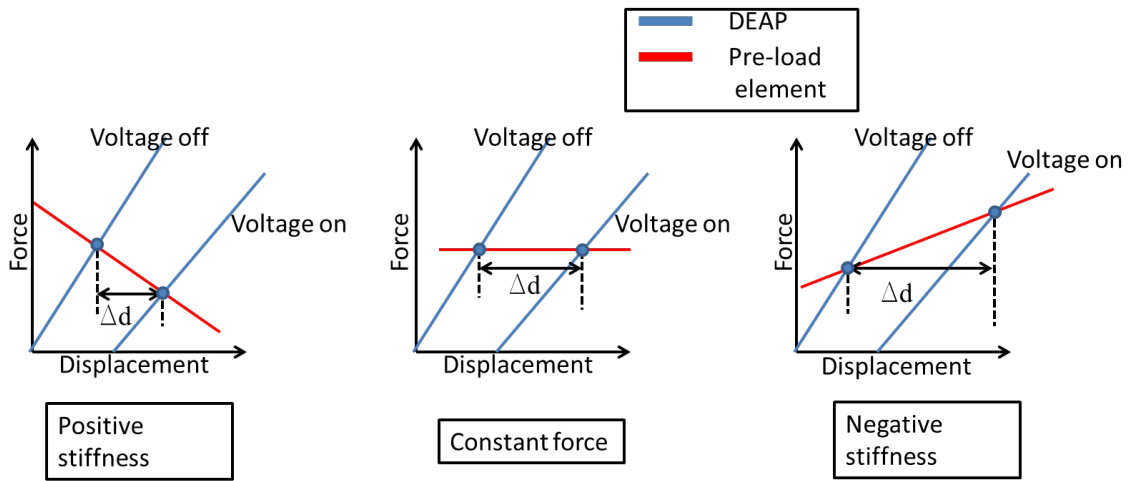
Figure 3.10: DEAP coupled to different pre-load elements. A positive stiffness spring (left), a constant force spring (middle) and a negative stiffness spring (right). Δd represents the output displacement of the DEAP actuator

The intersections between the pre-load curves and the DEAP on and off curves are the two equilibrium positions the actuator reaches during operation. The distance between the equilibrium points is the effective actuator output displacement. The graphs indicate that a negative stiffness pre-load element produces the highest stroke and that a constant force element produces more stroke than a positive stiffness element.

The theory behind the interaction between pre-load and the DEAP will be applied for the actuators built in this thesis. In the following chapters, an actuator with a positive stiffness pre-load element will be presented followed by an actuator with a constant force element. The two actuators will be characterized and compared.

3.6 Summary

A study on the effect of pre-strain (1) on actuator performance was conducted. The free displacement and blocked force response were measured at pre-strain values ranging from 0 to 15.3%. The results indicate the effects of pre-strain are more significant on the blocked force response than on the displacement response. Nevertheless, the results suggest an optimal axial pre-strain value of 12% or pre-stress of 53.3 KPa to enhance the performance of a DEAP actuator using the Danfoss Polypower material. In addition, a discussion on the types of preload and how they interact with the DEAP material was presented. It was shown that a negative stiffness pre-load coupled to the DEAP results in highest actuator displacement. The negative stiffness pre-load will not be covered in this thesis, but two actuators will be built using a positive stiffness and constant force pre-load element. Both actuators will be pre-strained to 12% and will be presented in chapter 4 and 5.

Chapter 4 Spring Roll Actuator

This chapter presents the development of a 1 DOF roll actuator with a positive stiffness pre-load element. The design of Actuator 2 follows the design of the "spring roll" discussed in chapter 1, which consists of a compressed coil spring packaged inside a DEAP roll. Using the knowledge gained in chapter 3, the DEAP film is pre-strained to 12-13% by a positive stiffness element. The design, working principle and actuator's response to voltage are presented here.

4.1 Spring Roll Design and Fabrication

The previous chapter found improvement in actuator performance when the DEAP film is mechanically pre-strained. To make a practical actuator, a clever way of maintaining the required pre-strain is needed. For the actuator presented here, a coil spring is used as the support structure that maintains the film pre-strained. The design consists of wrapping the DEAP material about a compressed spring and then releasing the spring to induce a pre-strain. Figure 4.1 shows the skeleton and the assembled actuator.
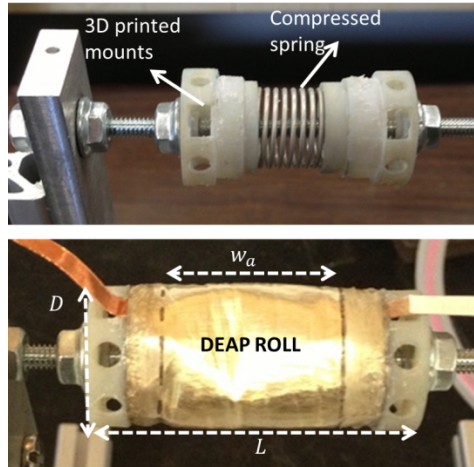
Figure 4.1 Skeleton of spring roll actuator (top) shows the compressed spring supported by 3D printed mounts. The material is then wound about the compressed spring (bottom) to complete the spring roll actuator.

The plastic mounting caps shown in figure 4.1 are 3D printed and designed to provide a good seating for the spring. The forces from the DEAP film are transmitted to the coil spring by gluing the DEAP film along the passive areas to the plastic mounts as explained in chapter 2.

As discussed in the last section of chapter 3, the lower the stiffness of the pre-load element, the higher the actuator displacement. The constraint on the value of the spring constant is the stiffness of the DEAP roll. The value of the coil spring constant needs to be equal or lower than the stiffness of the DEAP roll. Hence, tensile load tests were conducted to obtain the tensile force – axial displacement behavior of the DEAP roll similar to tests in section 3.4. The tensile force-displacement behavior is shown in figure 4.2. A linear fit to the data indicates a stiffness of 280 N/m.
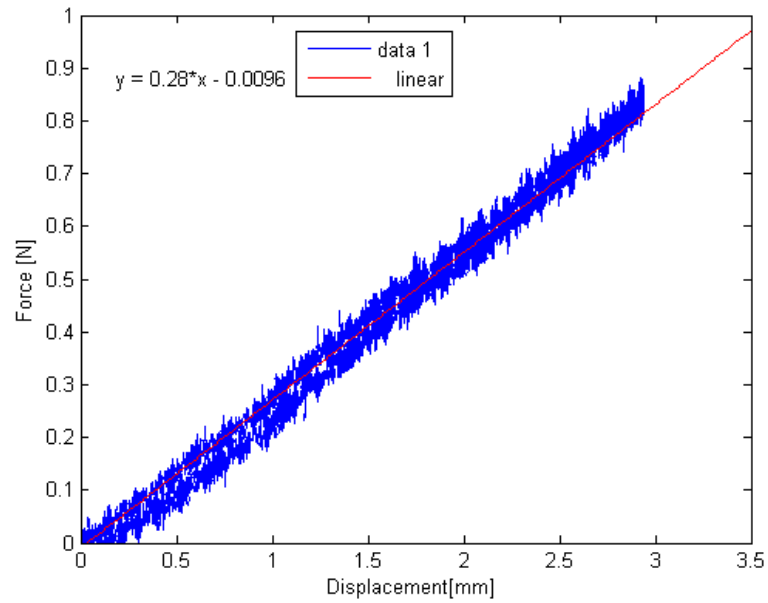
Figure 4.2: Tensile force - axial displacement behavior of DEAP roll used to extract the stiffness of the DEAP roll. Experimental data (blue) is plotted with linear fit(red).

Finding a commercially available coil spring with low stiffness is rather easy. However, this compromised the weight and sometimes the size of the actuator. The softer the spring, the more deflection it needs to reach the required pre-load hence making the coil spring long. Taking all of those factors into consideration, a spring was chosen. All final properties of the actuator are shown in table 4.1.

Table 4.1: Spring roll actuator characteristics

Spring Roll actuator properties			
Diameter (D)	Length (L)	Total mass (kg)	Spring constant of pre-load element
17 mm	50 mm	.0025	240 N/m
DEAP Roll Active geometric properties			
Active length (L_a)	Active Width (W_a)	Cross Sectional area $(A = L_a * t * 2)$	Stiffness
95 mm	25.5 mm	15.2 mm²	280 N/m

The chosen spring is compressed enough to provide a required preload of .81 N based on the 53.3 KPa pre-stress. On another note, it was desired for the actuator to be small in diameter. However, the diameter of the actuator is dictated by the diameter of the spring. Springs with smaller diameters were tested but they easily buckled during operation leading to actuator failure.

4.2 Spring Roll Actuator Principle of Operation

In order to explain the operation of the spring roll actuator, the force-displacement behavior of the coil spring and the DEAP film are plotted qualitatively in figure 4.3.
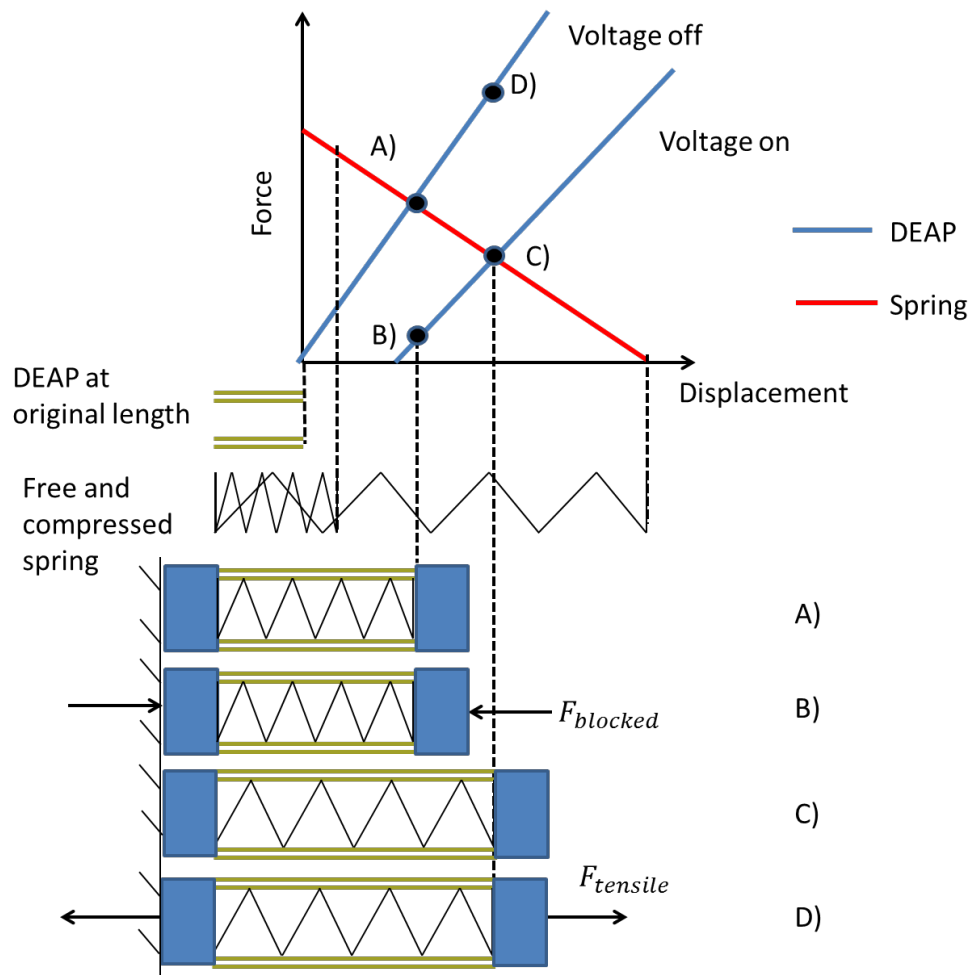
Figure 4.3: Spring roll actuator principle of operation. Four states are identified depending on the boundary conditions. A) and D) represent deactivated states while B) and C) represent active states.

From the activation and deactivation of the actuator, four different states can be identified depending on the boundary conditions. These states represent the following:

- (A): The DEAP film and spring are in force equilibrium while deactivated. The film is pre-strained by the compressed spring.

- (A) - (B): The actuator is activated with its ends blocked from movement. Upon activation, the film relaxes and releases the compressed spring. An external compressive force restricts the actuator from movement.

- (A) - (C): The actuator is activated with its ends free to move. The application of voltage causes the film to relax and release the compressed spring. The spring expands until the force of the spring and DEAP film reach new force equilibrium.

- (C) - (D): The actuator's ends are fixed and subsequently deactivated. A tensile force at the boundaries prevents the actuator from contracting.

The characterization of the actuator will consist in measuring the compressive forces in state (B) and the displacement of the actuator between (A) and (C).

4.3 Spring Roll Actuator Characterization

The quasi-static and dynamic behavior of the spring actuator is explored in this section. In particular, the free displacement and blocked force response are presented under DC and triangular waveform voltage activation. The actuator frequency and transient response are also presented.

4.3.1 Experimental Setup of Spring Roll Characterization

The test setup and experimental procedure discussed in chapter 3 are used to measure the blocked force and free displacement of the spring roll. Some modifications were done to the Labview code for the dynamic tests but the overall function of the code remained the same.

4.3.2 Spring Roll Stroke Results

The quasi-static stroke response of Actuator 2 is shown in figure 4.4. The actuator reaches a maximum stroke value of about .44 mm at 2500 Volts (maximum voltage) corresponding to a strain of 1.7%. Figure 4.5 shows steady state stroke for 2 cycles of the electrical loading at .1Hz, 1Hz, 10Hz, 25Hz and 50Hz. This test revealed that the maximum actuator stroke stays the same for frequencies up to 10Hz. The actuator stroke was expected to decrease because of the viscoelastic behavior of the material but one reason could be the small strain values achieved by the actuator upon activation. In addition, some harmonics appear in the 10Hz response but they become more obvious as the frequency is increased.
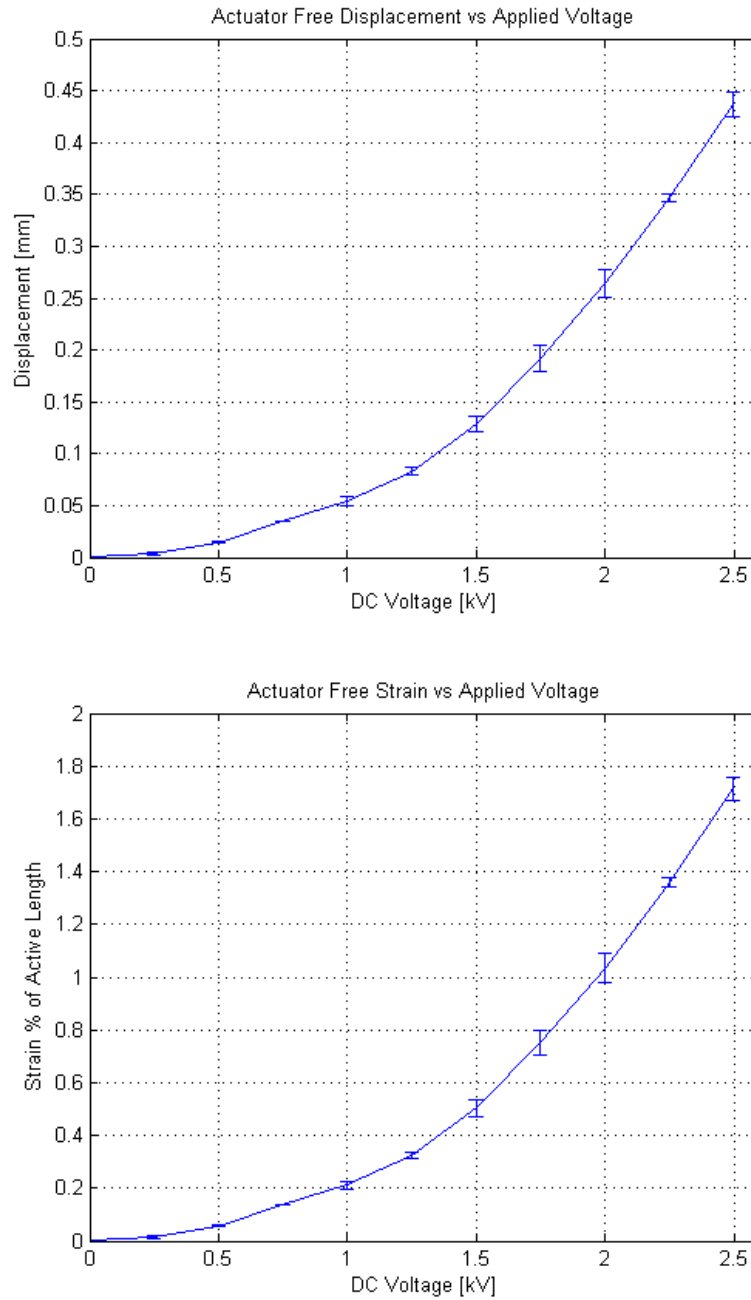
Figure 4.4 DC output from spring roll actuator: Actuator stroke (top) and actuator strain of active material (bottom)
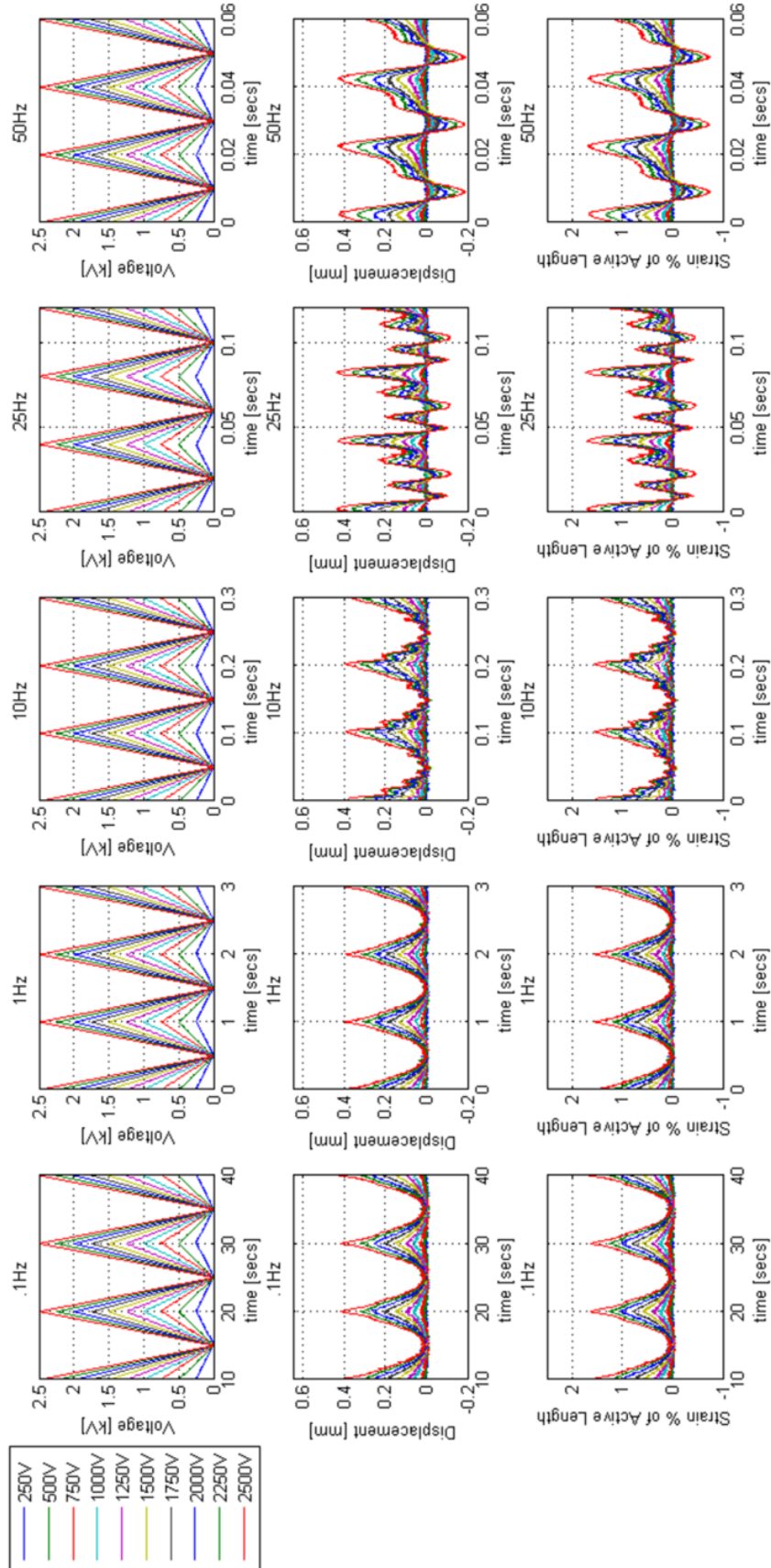
Figure 4.5 Spring roll response to cyclic triangular loading: Input voltage (top), output displacement (middle) and strain of active material (bottom)

4.3.3 Spring Roll Blocked Force Results

Figure 4.6 shows the quasi-static blocked force response of Actuator 2. The actuator reaches a maximum blocked force value of .26 N or 17KPa in terms of actuation pressure. The actuation pressure value is higher than the one achieved by Danfoss Polypower roll actuators [31] at the same voltage. The steady state blocked force response for 2 cycles of the electrical loading at .1Hz, 1Hz, 10Hz, 25Hz and 50Hz reveal similar trends seen in the stroke dynamic tests (see figure 4.7). However, the blocked force seems to decrease as the frequency increases past 10Hz.
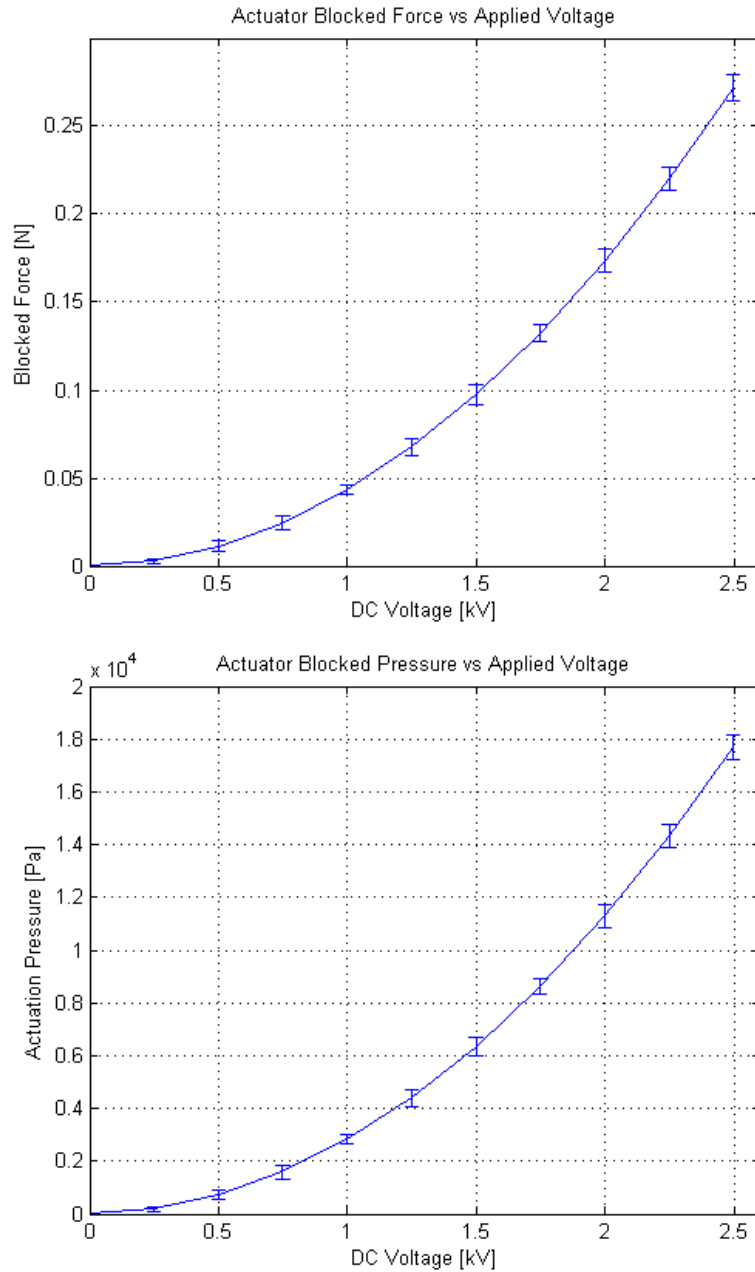
Figure 4.6 DC output from spring roll actuator: Actuator produced blocked force (top)

and actuator blocked actuation pressure (bottom)
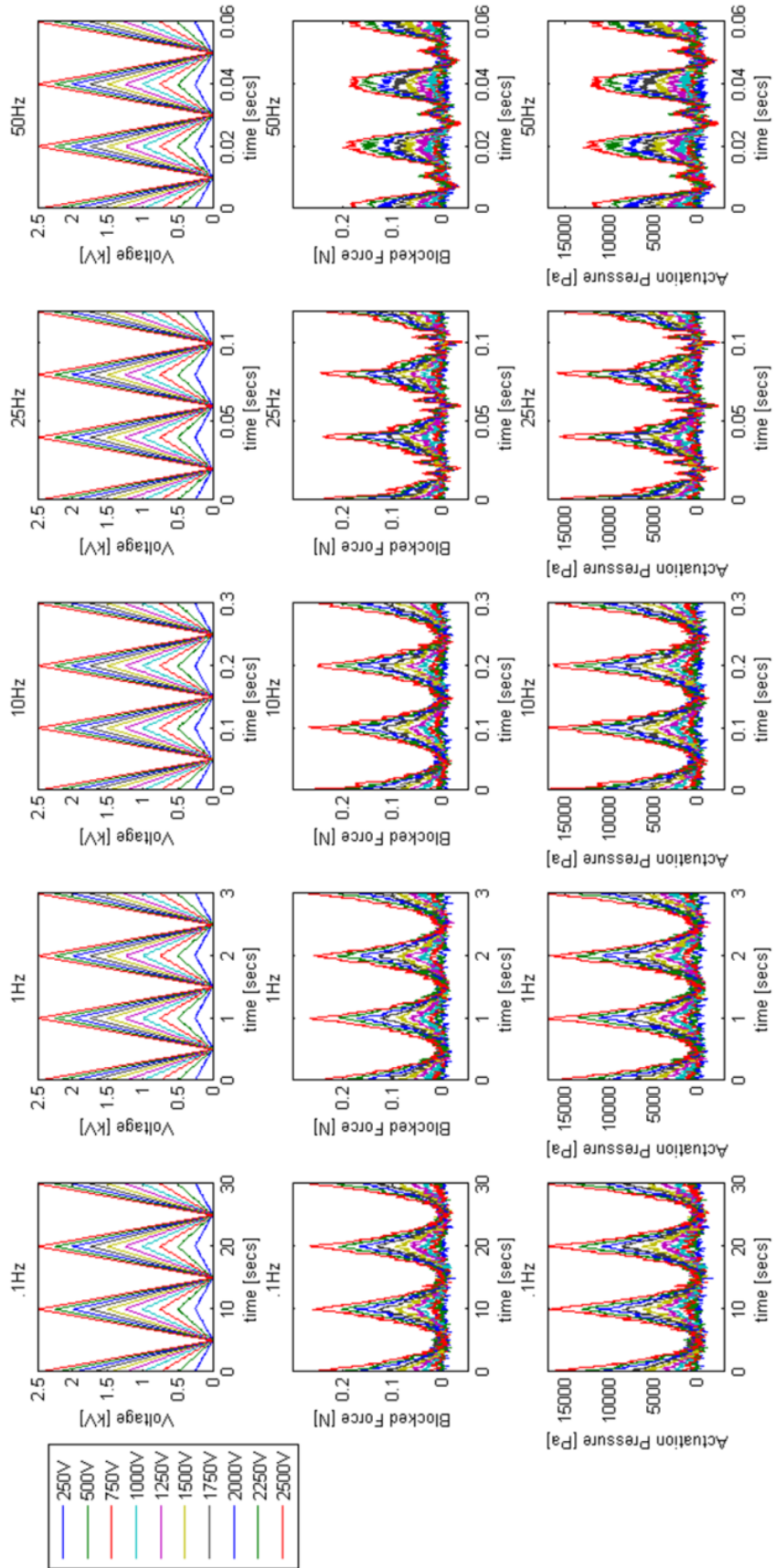
Figure 4.7 Spring roll response to cyclic triangular loading: Input voltage (top), blocked force (middle) and blocked actuation pressure (bottom)

4.3.4 Spring Roll's Transient and Frequency Response

Figure 4.8 shows the actuator's time response to a step input from 0 to 2000V without any external load. The actuator main transient parameters are summarized in table 4.2. Assuming the actuator is a second order damped harmonic oscillator, the natural frequency and damping of the system can be obtained.
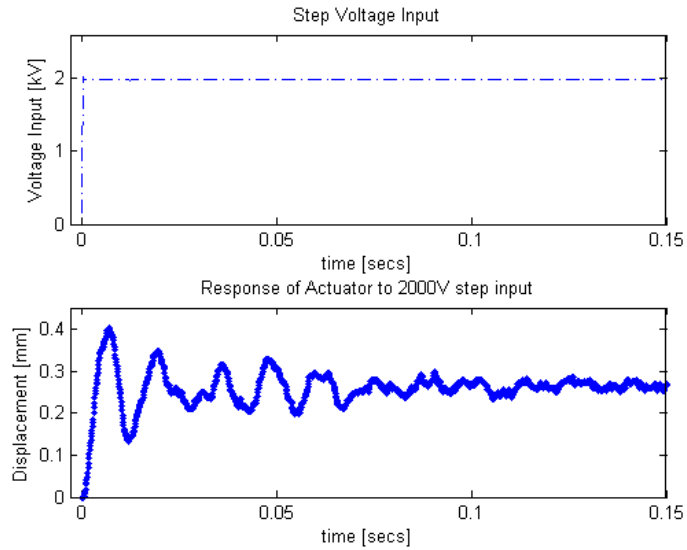
Figure 4.8: Spring roll response (bottom) to a 2000 V step input (top) under no load.

Table 4.2: Spring roll actuator step response parameters

Parameter	Value
Response time(peak time)	7.6 ms
Settling time	.22 s
Rise time	2 ms
Overshoot	52 %

A damped harmonic oscillator is described by equation 4.1 where ζ is the damping ratio and w_o the natural frequency of the system.

$$\frac{d^2x}{dt^2} + 2\zeta w_o \frac{dx}{dt} + w_o^2 x = 0 \qquad\qquad 4.1$$

Equation 4.2 is equivalent to equation 4.1 where m is the mass, k the stiffness, and c the damping of the system.

$$\frac{d^2x}{dt^2} + \frac{c}{m}\frac{dx}{dt} + \frac{k}{m}x = 0 \qquad\qquad 4.2$$

The natural frequency w_o and damping ratio ζ of a second order, under-damped system is given equation 4.3 and 4.4.

$$w_o = \sqrt{\frac{k}{m}} \qquad\qquad 4.3$$

$$\zeta = \frac{c}{2w_o} \qquad\qquad 4.4$$

The damping ratio can also be approximated by equation 4.5 where T_s is the settling time of the step response.

$$T_s = \frac{3.9}{\zeta w_o} \qquad\qquad 4.5$$

The mass of the system is composed of all the moving parts: the mass of the upper mount, the mass of the spring, and the mass of active and upper passive region. This added up to a total of about 1.8 mg. The stiffness of the DEAP roll was experimental found, 280 N/m (see figure 4.2) and that of the bias spring is 245 N/m. Adding the stiffness and plugging into equation 4.3, the approximate natural frequency of the spring roll actuator is 86.5 Hz. Using the estimated natural frequency and the settling time in table 4.3, equation 4.4 indicates the damping ratio is .03. Knowing the damping ratio allows the computation of the overall damping of the system given by equation 4.4. All calculated parameters are summarized in table 4.3.

Table 4.3 Summary of parameters of spring roll actuator based on 2nd order system assumption

Parameter	Value
Mass of moving part (m)	1.8 g
Total system stiffness (k)	525 N/m
Calculated damping of system (c)	35.45 N s/m
Calculated natural frequency (w_o)	86.5 Hz
Calculated damping Ratio (z)	.03

The electromechanical impedance (mm/V) as a function of frequency was investigated. A chirp voltage signal was generated in labview and applied to the spring roll actuator. A chirp signal is a sine wave that increases in frequency over time. The main inputs include starting and stopping frequencies and the time span of the wave. The test was conducted for two different drive voltages, 0 to 1kV (500V amplitude and 500V DC offset) and 0 to 1.5kV (750V amplitude and 750V DC offset). The chosen start and stop frequencies are 1Hz and 110 Hz respectively and span of the wave was set to 110 seconds. The results of these tests are shown in figure 4.9. The response shows a resonance peak at high frequencies and a resonance/anti-resonance pair at low frequencies. The locations of the peaks seem to shift at the higher voltage input. This can be party explained by the decrease in stiffness the DEAP material experiences upon activation. Recalling the working principles of the material: when a high electric field is applied, the thickness of the material decreases and the DEAP film expands. This change

in geometry results in a decrease in stiffness which shifts the location of the peaks in figure 4.9.
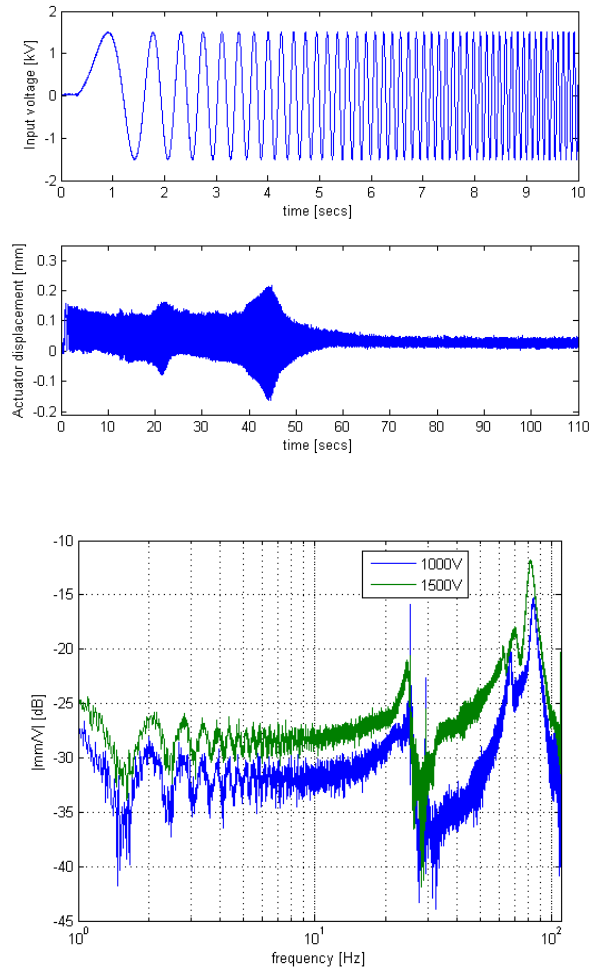
Figure 4.9: Ten seconds sample of the 110 seconds chirp signal (750V amplitude and 750V offset) (top) applied to DEAP actuator. Actuator output displacement response to chirp signal (middle). Magnitude of the fast Fourier transform of the output (mm) divided by input (V) as a function of frequency (bottom) for two chirp signals.

The resonance/anti-resonance pair at low frequencies can be explained by the electrical input exciting a mechanical resonance in the DEAP material. The resonance

peak at the higher frequency values represents the resonance of the entire system. Comparing the frequency of the peak furthest to the right at 1000 V and the calculated natural frequency shown previously, both frequency values are close. Table 4.3 shows the measured and calculated frequency values.

Table 4.4 Measured and calculated system resonance frequencies of spring roll actuator

Measured	Calculated
~ 82 Hz at 1500V	86.5 Hz
~ 85 Hz at 1000V	

4.4 Summary

This chapter focused on the development of a DEAP actuator coupled to a positive stiffness bias element, otherwise known as the spring roll. The experimental characterization shows that the compressed spring helps the actuator produce more force in addition to the gains due to pre-strain. The actuator blocking forces exceeded those from the pre-strain experiment while using the same active parameters. The maximum displacement response of .4 mm is rather low especially compared to the .6 mm displacement seen in the pre-strain studies. One possible explanation for the low displacement is the stiffer spring used in the actuator presented here compared to the bias spring used in the pre-strain study.

Chapter 5 Constant Force Biased (CFB) DEAP Actuator

Chapter 5 explores the development of a DEAP roll actuator coupled to a constant force biasing (CFB) element. A 12-13% pre-strain will be applied the DEAP film just like in the spring roll actuator discussed previously. The dimensions of the active areas in the DEAP sheets are kept the same from spring roll actuator and pre-strain studies in order to compare their behavior. The design, working principle and actuator's response to voltage are presented.

5.1 Constant Force Element Concept

Buckling is often thought as sudden structural failure of a member under compressive loads. But, analysis shows that the axial stiffness of a member under compression is significantly reduced when the load is higher than the critical buckling load [12] (see figure 5.1). As shown below, the nearly constant force region appears right after a beam buckles. This concept will be attempted to be used in the CFB element design.
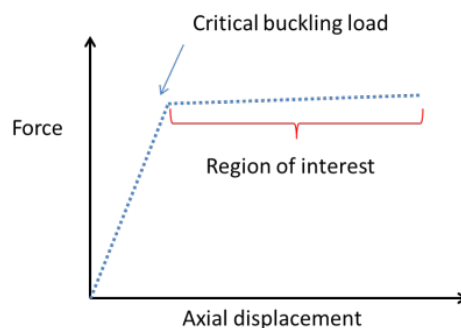
Figure 5.1Typical behavior of a beam compressed past the buckling load. Beam stiffness decreases after critical buckling load. As long as the stresses in the beam stay within the elastic region, the buckling deformations are reversible.

5.2 CFB DEAP Actuator Design

As mentioned in the last section, the concept of buckled beams will used in the design of a constant force bias (CFB) element and must exhibit the behavior shown in figure 5.1. The main design parameters of the CFB element include choice of material, geometry and boundary conditions. Initial iterations consisted of using steel spring beams with pinned boundary conditions. However, without the use of bearings, the pinned boundary conditions were poorly simulated which led to inconsistent post-buckling behavior. The need to keep the design simple, light weight and reduce the amount of moving parts was important. Hence, this gave rise to the CFB element shown in figure 5.2. The design shown consists of two carbon fiber beams with fixed boundary conditions. The element will be externally attached to the DEAP roll by using small bolts as shown.
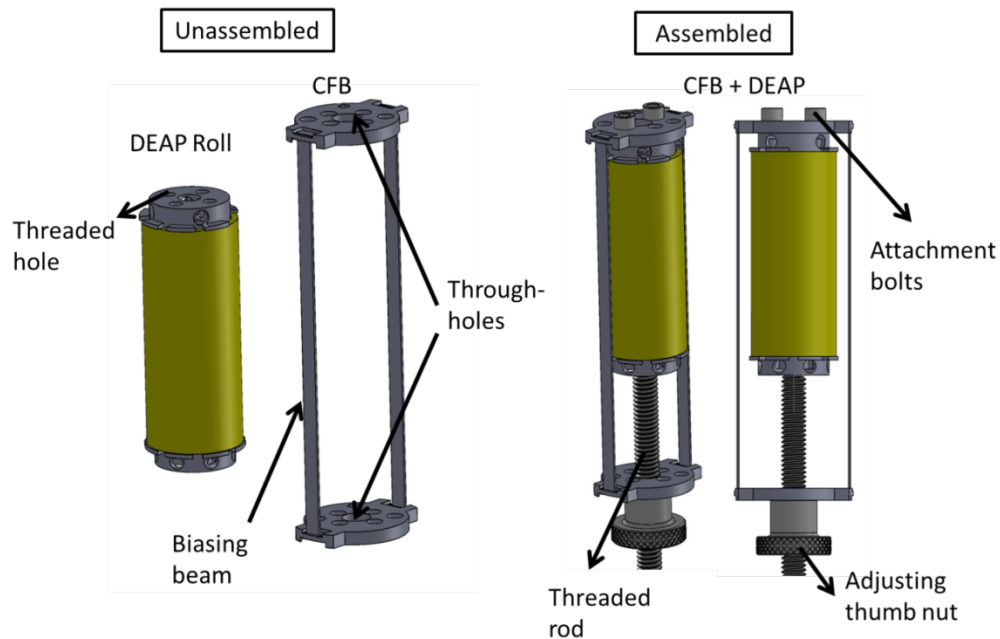
Figure 5.2 CAD drawing of CFB actuator prototype. CFB element and DEAP roll unassembled view (left). Assembled CFB actuator (right).

A threaded rod and a thumb nut will serve as the mechanism that couples the compression load on the beams to the tensile load on the DEAP roll. Figure 5.3 describes the procedure of supplying the pre-stretch to the DEAP roll using the CFB element.
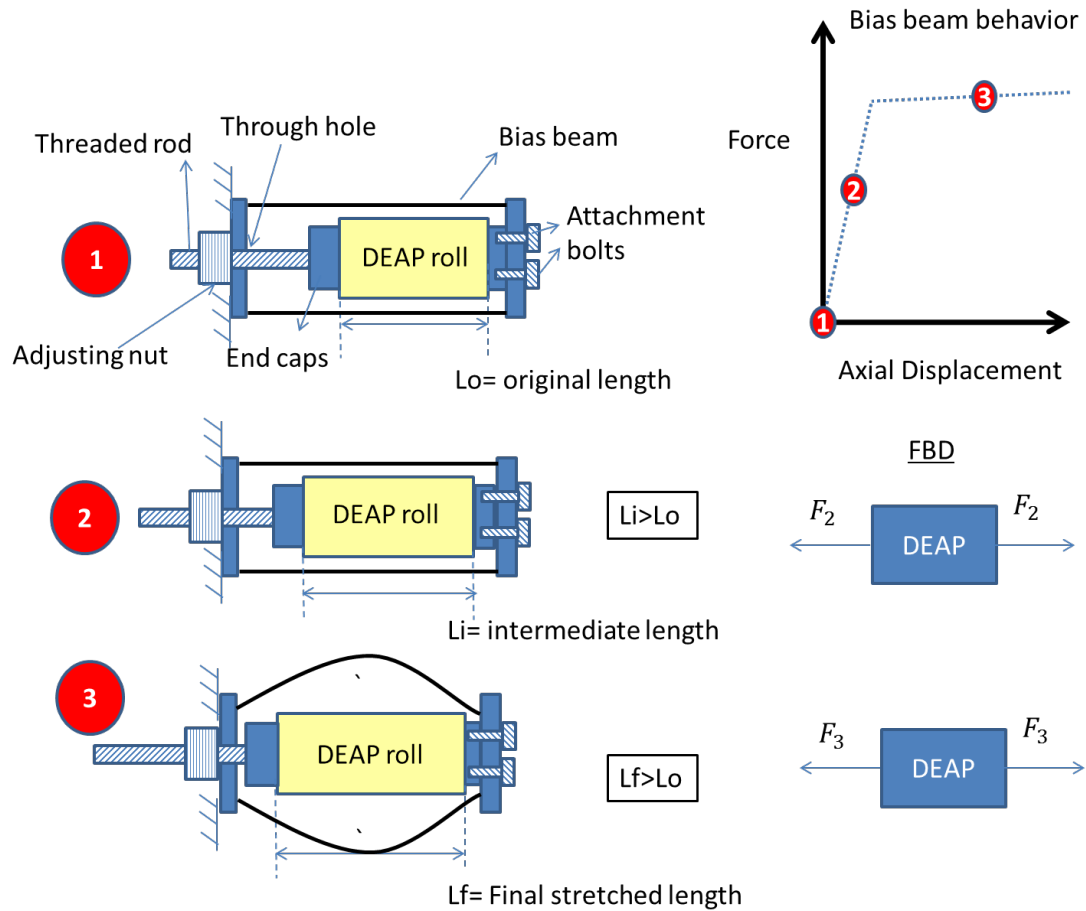
Figure 5.3 Pre-strain supply steps by CFB element. DEAP roll and beam deformation schematic (left). Path of beam behavior at every step (right)

At stage 1, the DEAP roll and the CFB element are not under load. At stage 2, the adjusting nut has been turned a couple of times clockwise putting the DEAP roll under tension due to the reaction loads of the beams. Then the nut is turned until load on the DEAP passes the critical buckling and onto stage 3. At this point the beams have deformed out of plane and the actuator is within the constant force region. Also, it is

important to know that the actuator must work far enough from the critical buckling point to prevent the beams from unbuckling during activation.

The Euler buckling formula is used to size the beams in the CFB element. For a fixed-fixed beam, the critical buckling load is given by equation 5.1.

$$P_{cr} = \frac{4*\pi^2*E*I}{L_b^2}$$
5.1

Pcr= Buckling load

E= Young's Modulus

I=area moment of inertia

L_b=beam length

P_{cr} is substituted in by one half the desired pre-load since there are two beams in the CFB element. The Young's modulus of the composite carbon fiber was experimentally found to be about 160 GPa (see appendix C). The length of the beams is partly constrained by the length (L) of the DEAP roll and the amount of pre-stretch (ΔL) desired (see figure 5.4). Hence, the length of the beams is chosen to be slightly higher thanL_{min}as seen in figure 5.4. The thickness of the beam is known since a single lamina of carbon fiber composite was used. Therefore, the only variable being calculated for is the width of the beams.
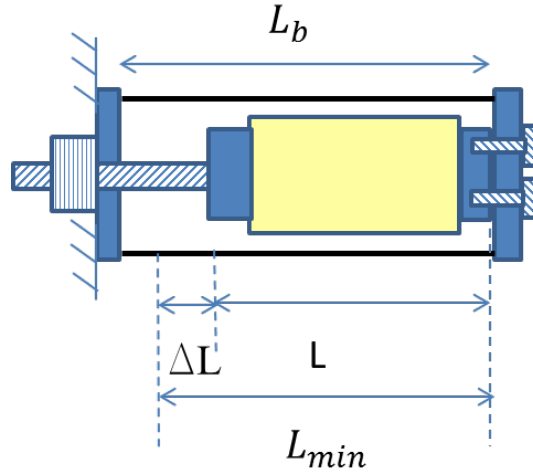
Figure 5.4: Schematic of CFB DEAP actuator showing the constraints on beam length. The value of L_b needs to be higher than L_{min} in order for the mechanism to work.

The same material active dimensions used in all previous actuators are used in the CFB actuator. This means the pre-load requirement for a pre-stress of 53.3 KPa stays as .81 N. Hence, using this pre-load value and a chosen beam length of 60 mm, the width of the carbon fiber beams are determined. A summary of the parameters of the CFB element prototype is shown in table 5.1.

Table 5.1: Parameters of CFB element prototype

Required Preload (P_{cr})	DEAP roll Length (L)	CF laminate thickness	Required Pre-stretch (ᴅL)	Chosen beam length (L)	Calculated beam width
.81 N	45 mm	0.1 mm	3.5 mm	60mm	2.6 mm

The load –displacement characterization of the CFB element was performed. This was done by mechanically controlling the displacement of one side of the beam while measuring the compressive force and displacement.

The displacement was controlled by a translation stage attached to one side of the CFB element while the other side is pushed against a beam type load cell (Futek Lb200) (see figure 5.4). The laser and DAQ system is the same as in chapter 3.The beam is compressed to 3.5 mm and its response is shown figure 5.5.
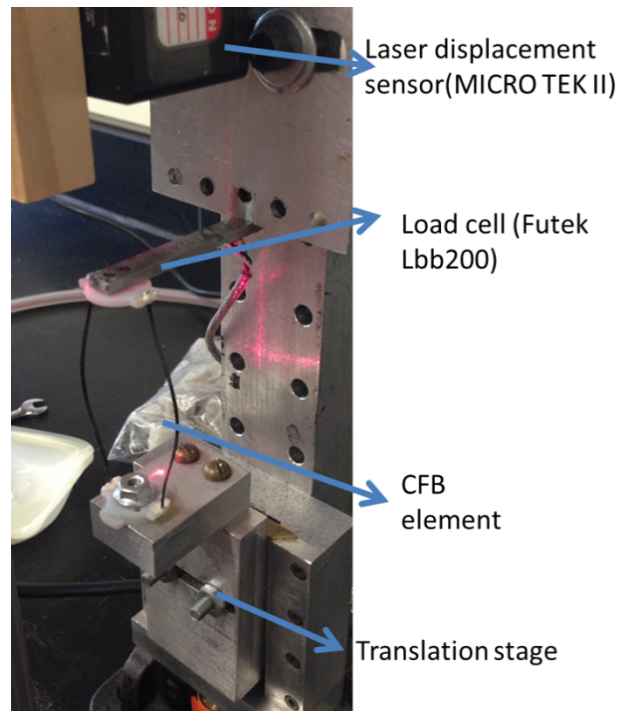
Figure 5.5: Experimental setup of CFB element characterization. The sledge of the translation stage moves up to and compresses the CFB element against the load cell. The displacement of the sledge is measured by a laser and the compressive force by the load cell.
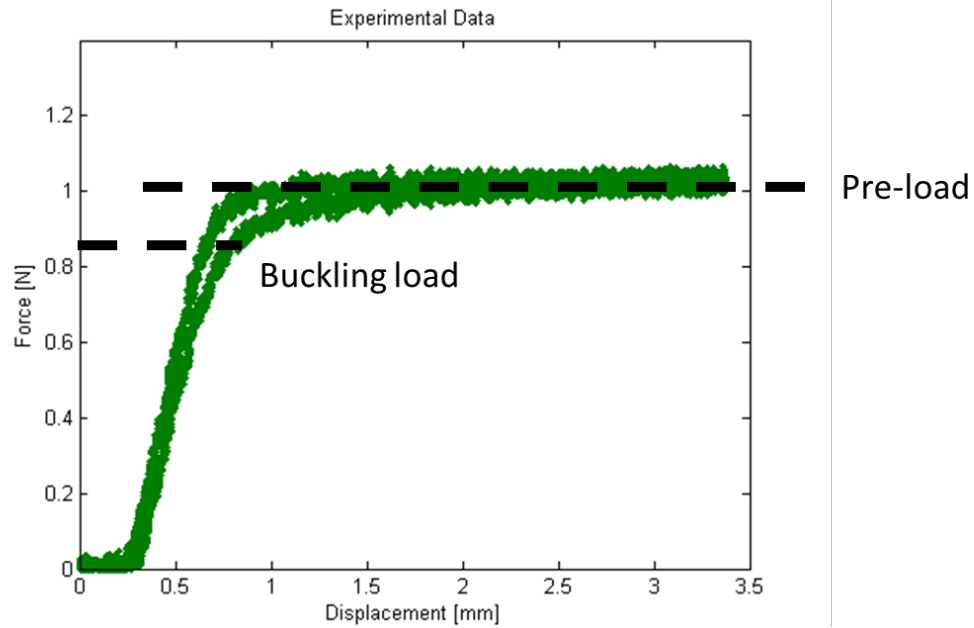
Figure 5.6 Compressive load vs. axial displacement behavior of CFB element. The buckling occurs when the compression force is about .83 N and the constant load region has a value of about 1 N.

The behavior seen in figure 5.5 follow what was expected in section 5.1. The CFB element constant force value is roughly 1 N and its buckling load about .83 N. The calculated pre-strain due to the 1 N pre-load is calculated to be about 13%.

5.3 CFB Actuator Principle of Operation

The CFB DEAP actuator goes through all 4 stages explained in section 4.2. The difference is that the force-displacement behavior of the bias spring now has zero slope (see figure 4.3) and the distance between state (A) and (C) is larger. Theoretically speaking, the displacement of the actuator is increased.

5.4 CFB Element Fabrication and Actuator Assembly

The DEAP roll is manufactured the same way described in chapter 2. The end mounts were modified and sized down to keep the actuator small. The attachment bolts are 2-56 in size and the threaded rod is 8-32 in size. The carbon fiber composite was made using a hand lay-up process and then cut to size using a diamond saw cutter. The beams were then fined tuned to size with sand paper. Using the high accuracy of the 3D printer, an assembly tool was built. Figure 5.6 shows some of the assembly steps of the CFB element. The assembled DEAP roll and CFB element is shown in figure 5.7.
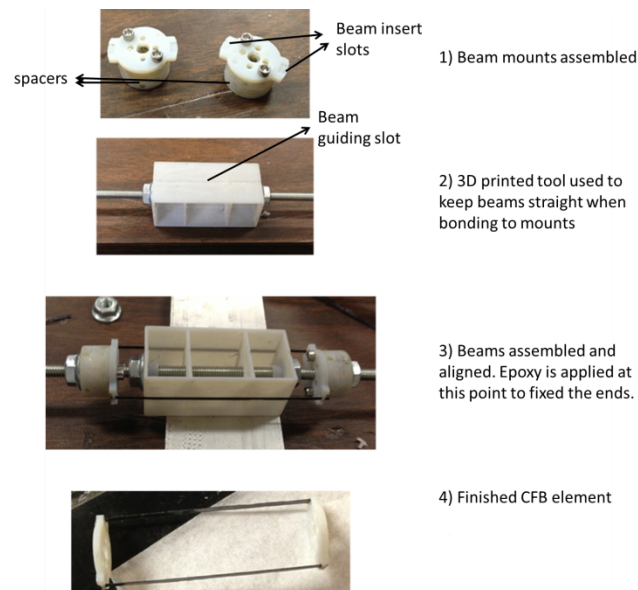
Figure 5.7 CFB element assembly parts (1-4). The beam mounts are attached to round 3D printed spacers by screws (1). A guiding tool used to align the beams is mounted on a threaded rod through concentric threaded holes (2). The spacers with the beam mounts are threaded into the rod and set apart based on the beam length. The beams are inserted and high strength epoxy is used to fix their ends (3). The CFB element is removed after the epoxy has cured overnight (4).
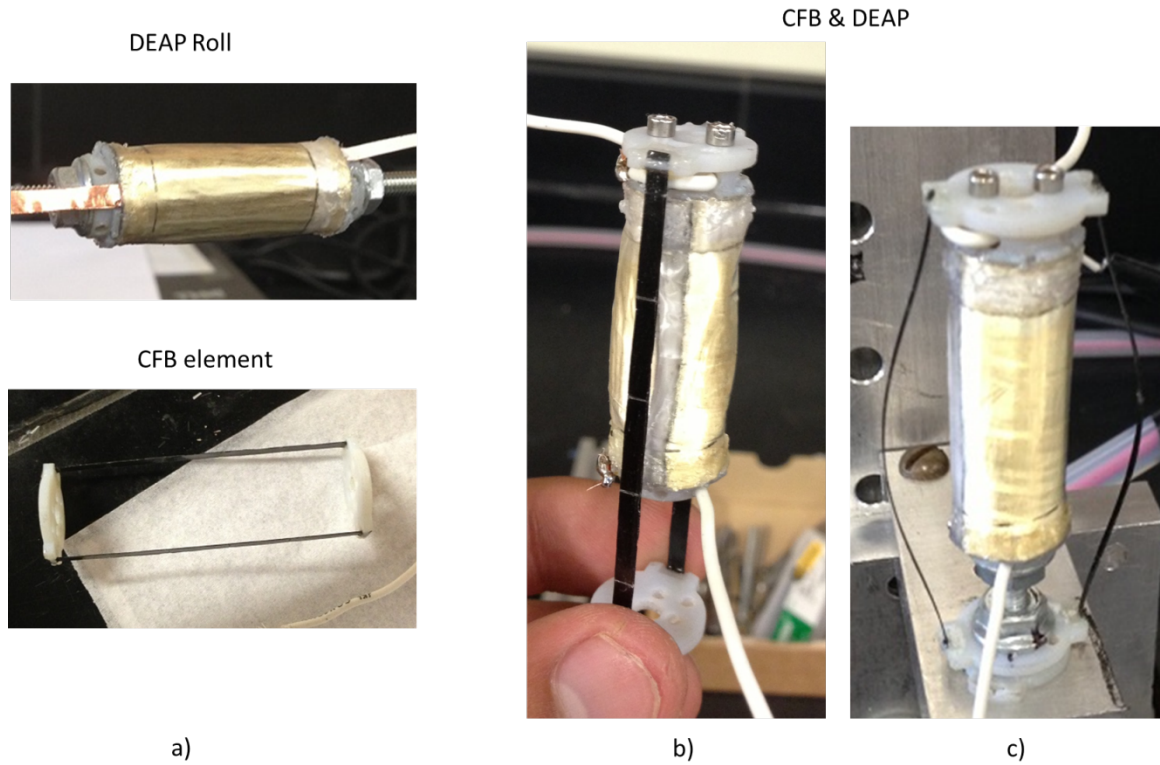
Figure 5.8 Assembly of CFB actuator prototype: a) the DEAP roll and CFB element separate views b) View of DEAP roll mounted to CFB element (no pre-strain supplied). c) View of operational configuration of CFB DEAP actuator (pre-strain applied)

5.5 CFB Actuator Characterization

The same tests conducted for the spring roll actuator are also performed for the CFB DEAP actuator. The experimental results presented will be compared to the spring roll actuator.

5.5.1 CFB Actuator Stroke Results

The quasi-static results indicate the actuator reaches a maximum stroke value of about .6 mm (2.3% strain) at 2500 Volts (see figure 5.8).This is a 25% increase in strain/stroke performance compared to the spring roll actuator. Figure 5.9 shows 2 cycles of the steady state stroke for the electrical loading rates of .1Hz, 1Hz, 10Hz, 25Hz and 50Hz. The test results indicate the stroke starts to gradually decrease at frequencies higher than 10 Hz. This can partly be explained by the unbuckling of the beams when the frequency hits the resonance/anti-resonance peaks that the frequency tests picked up in both the spring roll actuator tests and in this actuator as it will be shown later.
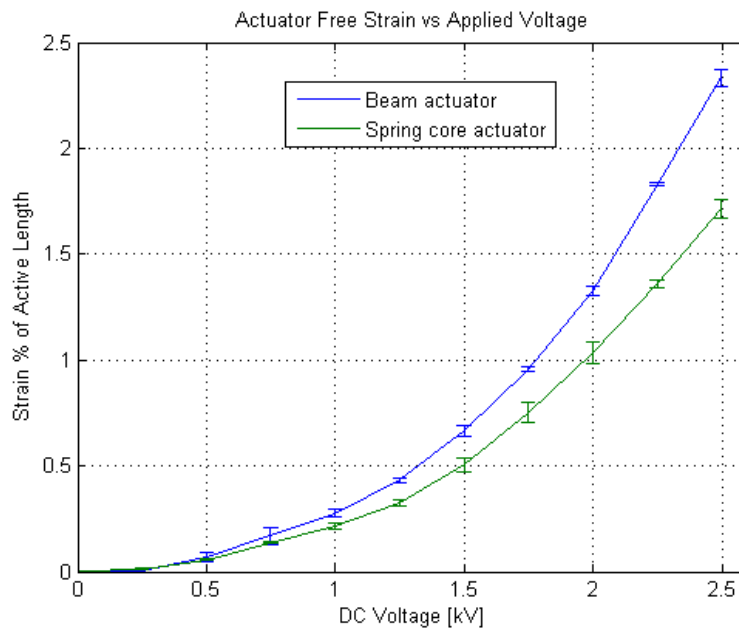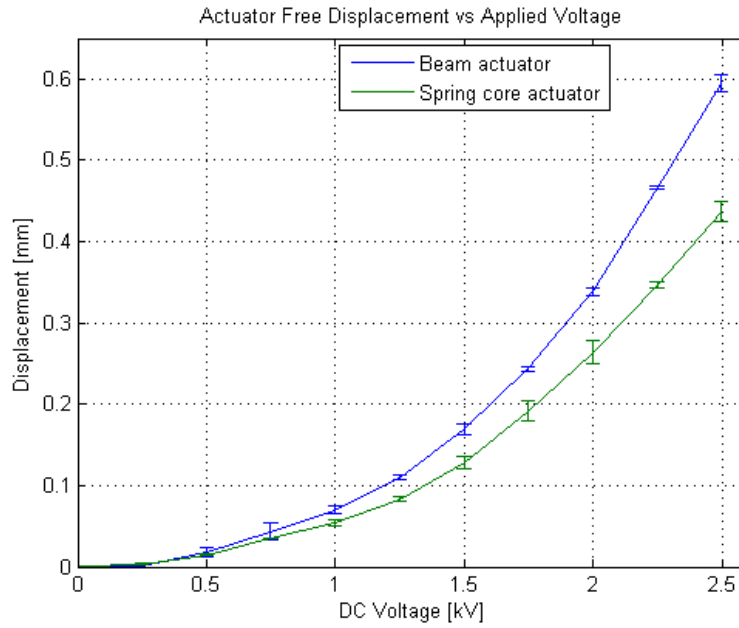
Figure 5.9 DC output from CFB DEAP actuator (blue) compared to the spring roll

actuator (green): stroke (top) and strain of active material (bottom)
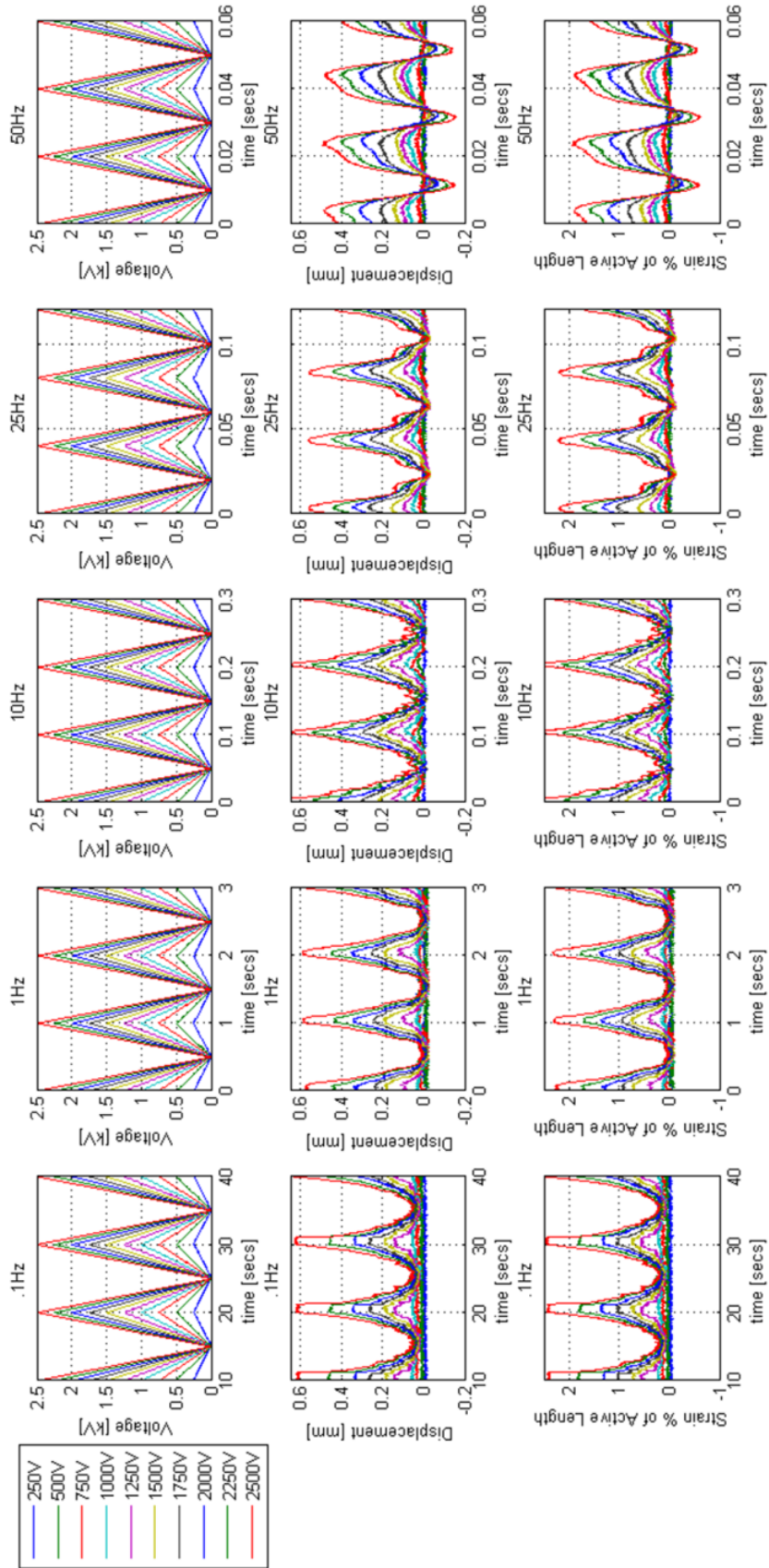
Figure 5.10 CFB DEAP actuator response to cyclic triangular loading: Input voltage (top), output displacement (middle) and strain of active material (bottom)

5.5.2 CFB Actuator Blocked Force Results

Figure 5.10 shows the quasi-static blocked force response. The actuator reaches a maximum blocked force value of about .2 N (14kPa actuation pressure). This result compared to the spring roll actuator is a 35% decrease in blocked force. The dynamic loading tests shown in figure 5.11 indicate the actuator maximum blocked force stays the same up to 50 Hz.
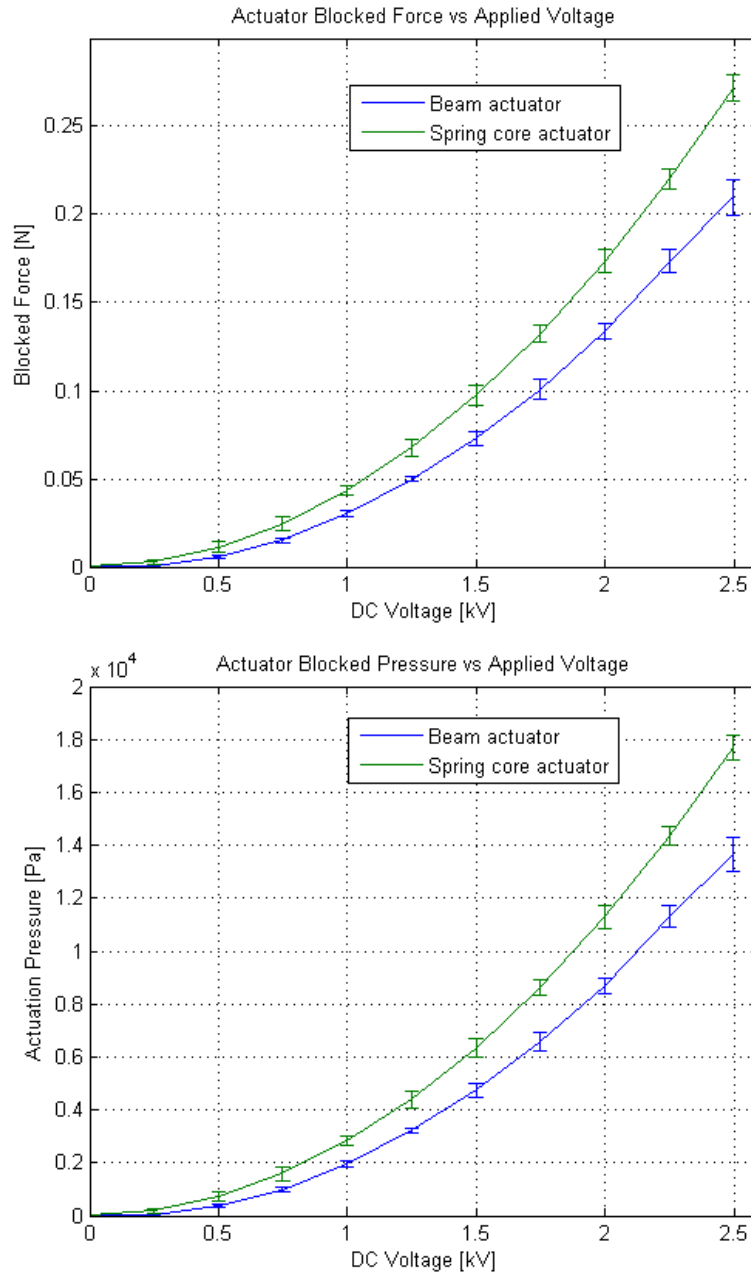
Figure 5.11 DC output from CFB actuator (blue) compared to the spring roll (green):

Actuator produced blocked force (top) and actuator blocked actuation pressure (bottom)
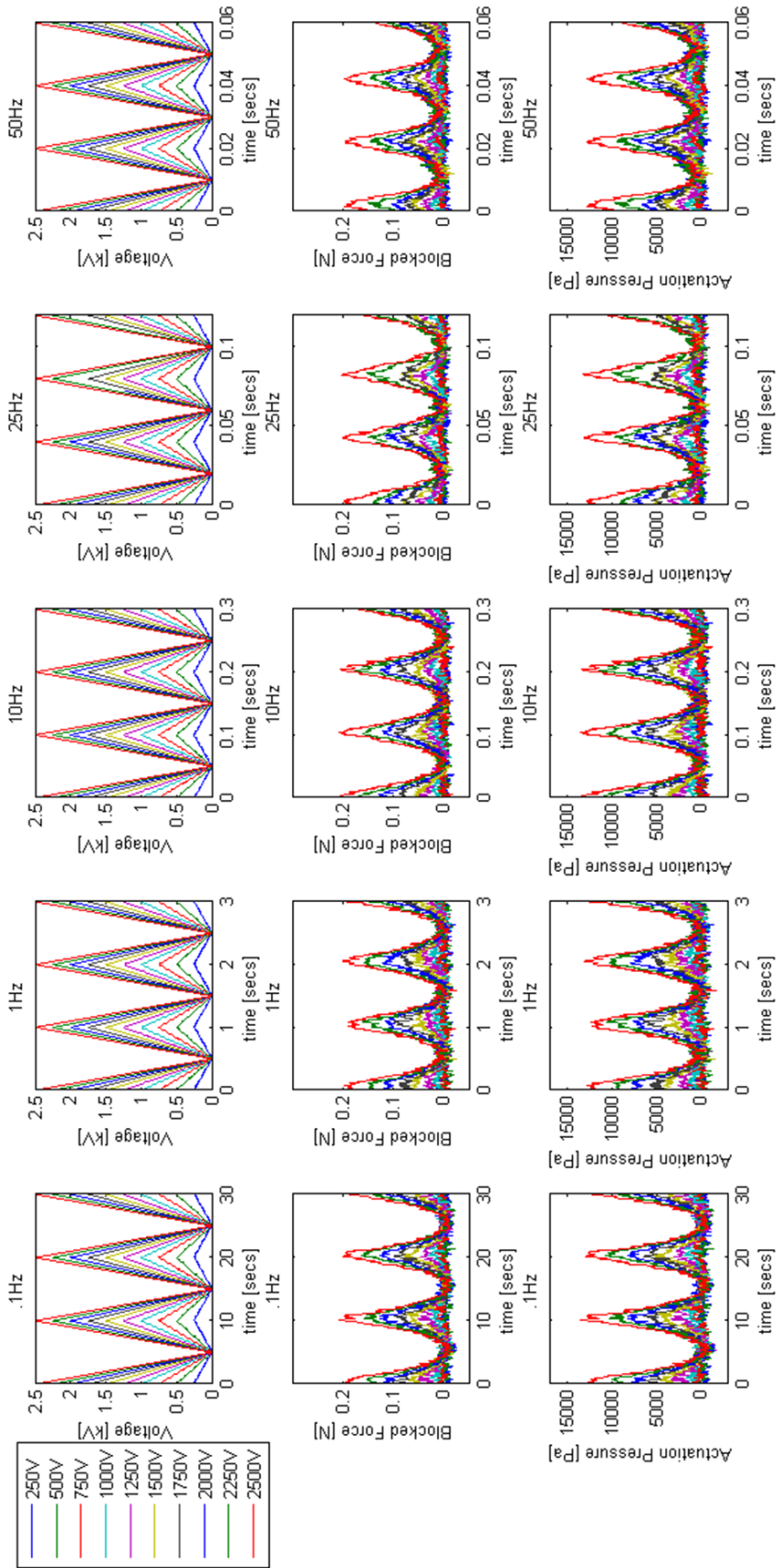
Figure 5.12 Spring roll response to cyclic triangular loading: Input voltage (top), blocked force (middle) and blocked actuation pressure (bottom)

5.5.3 CFB Actuator Transient and Frequency response

The actuator's time response is measured at the same voltage step used for the spring roll actuator test. The same test is repeated 3 times but only one is presented. The main transient parameters are summarized in table 5.2. The response time of the actuator has decreased by about 10% and can be attributed to the low mass of the CFB element.
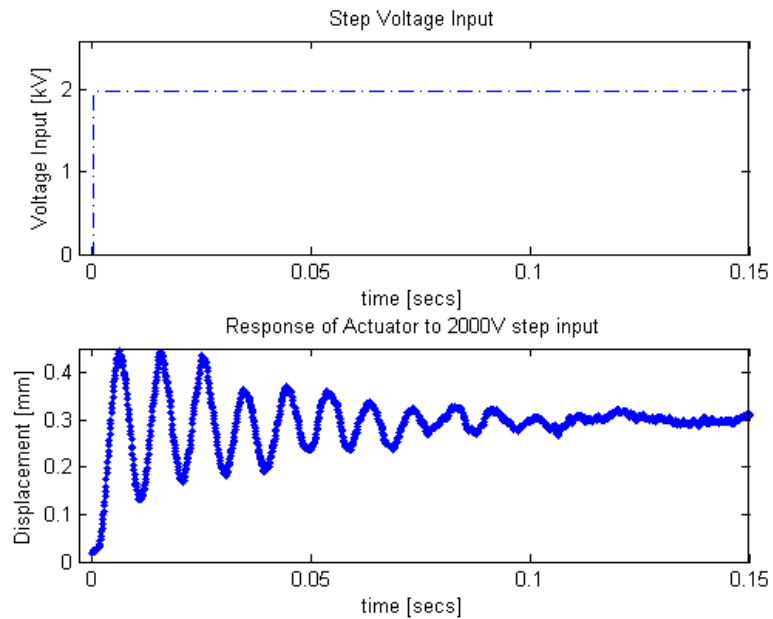
Figure 5.13 CFB actuator displacement response (bottom) to a 2000 V step input (top) under no load.

Table 5.2: CFB DEAP actuator response parameters to a 2000 V step input

Parameter	Value
Response time(peak time)	6.8 ms
Settling time	.2 s
Rise time	2 ms
Overshoot	49 %

The same calculations performed in section 4.3.5 are performed here to obtain the natural frequency and damping of the CFB DEAP actuator. The stiffness of the system is mostly given by the DEAP roll and the mass of the moving part has decreased because of the light weight composite CFB element. The calculated parameters are listed in table 4.3.

Table 5.3 Summary of parameters of CFB DEAP actuator based on 2nd order system assumption

Parameter	Value
Mass of moving part (m)	.9 g
Total system stiffness (k)	290 N/m
Calculated damping of system (c)	35 N s/m
Calculated natural frequency (w_o)	88 Hz
Calculated Damping Ratio (z)	.03

As in the spring roll actuator test, a chirp signal at two voltage levels (0 to 1kV and 0 to 1.5kV) and start/stop frequencies (1Hz to 110Hz) was applied to the CFB actuator. The electromechanical impedance amplitude response (|mm/V|) was obtained by taking the fast Fourier transform of the division between output (displacement) and input (voltage). The magnitude (|mm/V|) of the Fourier transform is shown in figure 5.13. The response of the spring roll is also shown for comparison.

As shown in figure 5.13, the location of the peaks shifts to the left with voltage increase. This supports the explanation given in chapter 4 that the stiffness of the material decreases when voltage is applied. In addition, the resonance/anti-resonance pair seen in

the spring roll response also appears in the CFB actuator response. As discussed previously, the origin of this resonance/anti-resonance pair is due to the electrical input exciting a mechanical resonance in the DEAP material.

Similarly, the resonance frequency of the system is thought to be captured. This is the furthest peak to the right of figure 5.13a. The resonance frequency was calculated previously assuming a second order system and its value is compared to the measured values in table 5.4. The theoretical value is close to the measured values indicating the actuator follows the behavior of an under-damped harmonic system.

Table 5.4 Measured and calculated system resonance frequencies of CFB DEAP actuator

Measured Resonance	Calculated-Theoretical Resonance
~ 86 Hz at 1500V	87.9 Hz
~ 88 Hz at 1000V	
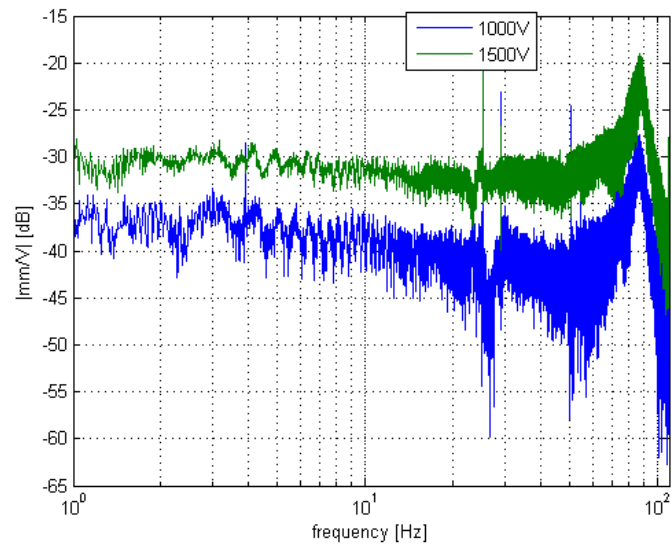
a)
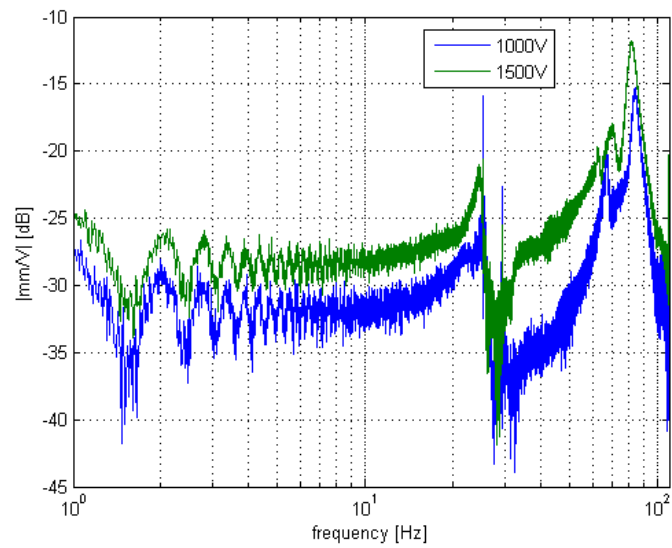
b)

Figure 5.14: Magnitude of the fast Fourier transform of the output (mm) divided by input (V) as a function of frequency for two chirp signals (1000V p-p (blue), 1500V p-p (green)). The response of the CFB actuator is shown at a) and the spring roll at b).

5.5.4 Spring Roll and CFB Actuator Work Potential

The work potential of the spring roll and CFB actuator is evaluated at voltages that range from 500V to 2500V. The work potential is the area under the actuator output force-displacement curve as shown in figure 5.14. The experimental setup used for this experiment is shown in figure 5.15 and is similar to figure 3.4 in chapter 3.

Starting with the actuator restrained from movement, voltage is supplied to the DEAP (point 1 on figure 5.14). At this point the actuator produces the most force, otherwise known as the blocked force. Then, the actuator is allowed to displace by moving the translation stage sledge up while measuring the output force (point 2 and 3 from figure 5.14). The point where the actuator no longer experiences the compressive reaction force of the translation stage is the free-displacement condition
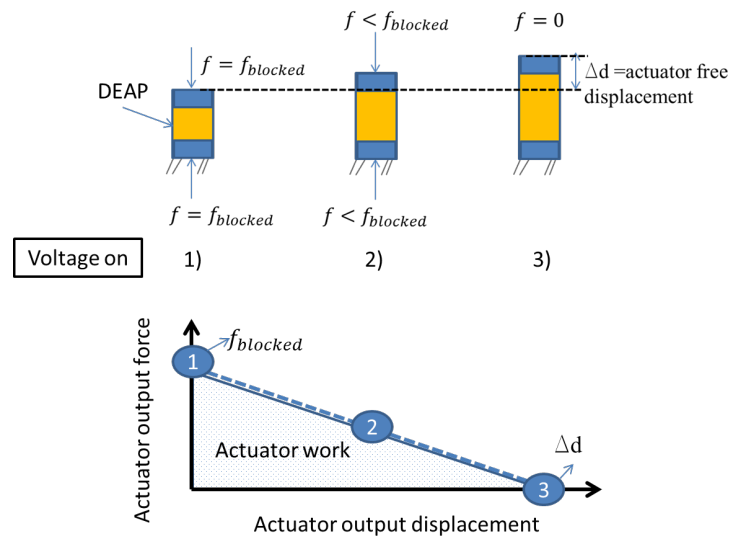
Figure 5.15 Schematic of actuator load line. 1) Actuator zero displacement, max force produced (blocked force). 2) Actuator allowed to displace but blocked from full elongation 3) Actuator is free to displace (max displacement or free displacement).
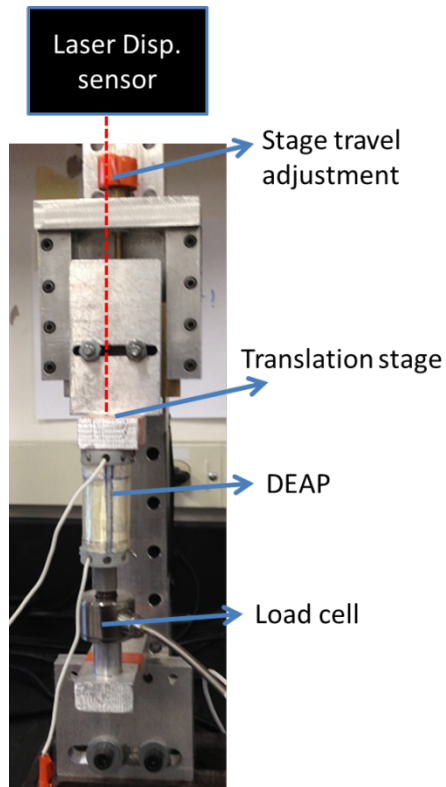
Figure 5.16: Experimental setup for work potential evaluation with main components labeled.

The force-displacement curves of both actuators are shown in figure 5.16. A linear approximation was fitted to the experimental data. The curves are consistent with the experimental results analyzed previously. It shows the gain in displacement with the CFB element but also the decrease in blocked force.

The work potential graphs are shown in figure 5.17. As shown, the spring roll actuator has a higher work potential than the CFB actuator for every voltage tested. This indicates that the decrease in blocked force is more substantial than the increase in stroke in the CFB actuator.
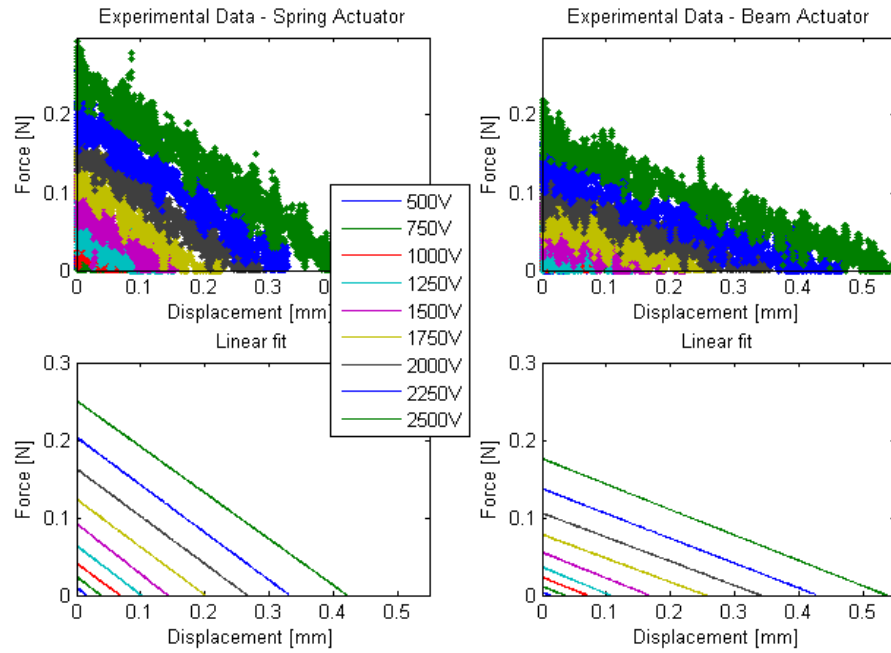
Figure 5.17 Experimental (top) and fitted (bottom) output force vs. displacement curves at different voltage levels for the spring roll (left) and CFB (right) actuator.
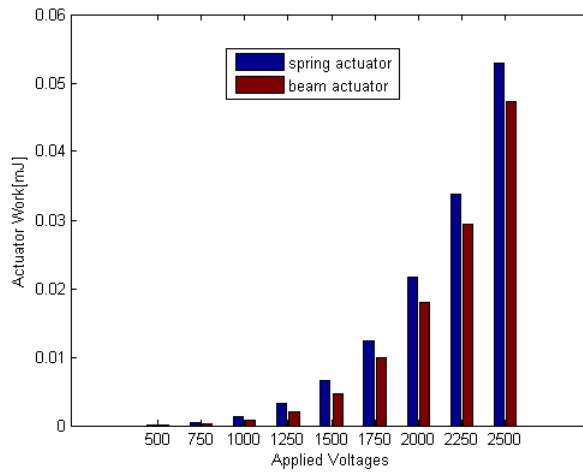
Figure 5.18 Work potential of spring roll (dark blue) and CFB actuator (dark red) for voltages ranging from 500V to 2500V

5.6 Summary

A prototype of a DEAP actuator with a constant force bias (CFB) element was developed. The concept of buckled beams was applied to the fabrication of the element. The beams are made out of carbon fiber to reduce the moving mass of the actuator. The fabrication and assembly of the CFB element was facilitated by 3D printed tools.

Compared to the spring roll, the impact of the CFB element is demonstrated in the increase of actuator stroke. As hypothesized at the end of chapter 3, the use of a constant force pre-load element helped increase the stroke produced by the actuator. On the other hand, the CFB actuator produced much less blocked force which can be attributed to the very low stiffness of the pre-load element. When the work potential was evaluated, it was found that the spring roll actuator outperforms the CFB actuator.

Chapter 6 Conclusions

The work presented in this thesis investigated the development of a roll Dielectric Electro Active Polymer actuator and different methods to maximize its performance. The DEAP material used in this research is a special film with a corrugated surface that allows expansion in only one planar direction.

First, the fabrication steps and tools needed to build an elemental roll actuator were presented in detail. This was followed by an investigation on the effects of pre-strain/pre-stress on the DEAP material. In this study, it was found that material performance is enhanced with a 12-13% pre-strain or 53.3 KPa pre-stress.

The interaction between a pre-strain element and the DEAP actuator was then discussed and it was shown how different types of pre-loads can increase the displacement output of an actuator. This led to the development of two actuators with different biasing elements: a positive stiffness biased (PSB) actuator otherwise known as the spring roll and a constant force biased (CFB) actuator.

The PSB actuator consisted of winding the DEAP film about a compressed coil spring which was released to pre-strain the film. The CFB actuator uses the concept of buckling to apply a constant force pre-load on the material. The characterization was conducted in terms of the actuator's stroke and blocked force capabilities. The main points drawn from the experimental results indicate that the CFB actuator produced more stroke than the spring roll at all voltage levels. On the other hand, the spring roll produced more blocked force than the CFB actuator. The increase in stroke is explained by the working principles between the pre-strain or pre-load element and the DEAP material covered at the end of chapter 3. The higher blocked force is attributed to the

stiffer pre-strain element used in the PSB actuator. Hence, it was concluded that the stiffer the pre-load element is, the higher the produced blocked force. Similarly, the softer the pre-load element is, the higher the stroke produced.

The work potential of both actuators was evaluated. The spring roll actuator outperformed the CFB device at all voltage levels. This indicated that the gains in blocked force when using a stiff pre-load element are more substantial than the gains in stroke achieved by a constant preload.

Appendix A

Temperature Tests

A study on the effects of temperature on actuator performance is attempted. A thermal test bench is constructed in order to subject the DEAP actuator to a high temperature environment. The material manufacturer indicates the ambient temperature of the material should be between -40°C and 100°C (-40°F and 212°F), however, it would be interesting to explore how the actuator actually performs at around these temperatures.

As shown in figure A.1, the thermal test bench consists of four heat lamps, four regular light bulbs and reflective aluminum foil to create a high temperature environment. Each bulb has its own switch hence allowing different temperature settings.

During experiments, the actuator is placed inside the test bench while covered by a metal tube painted with light absorbing paint (see figure A.1.c). When the bulbs are turned on, the tube absorbs all of the light and heat emitted by the bulbs. As a result, the temperature inside the tube increases and a high temperature environment is created.

A type K thermocouple is run through the metal tube and its measuring junction placed around the actuator location. The thermocouple voltage is converted to temperature by an Omega HH802U thermocouple thermometer. A laser displacement sensor is placed at the bottom of the thermal chamber and points to the moving actuator (see figure A.1 d.).

The actuator was tested at 4different temperature levels starting from room temperature (70°F) up to 155°F. Although higher temperatures could be tested the displacement readings become erratic and misleading at higher temperatures. This is

partly explained by the thermal expansion of the actuator test stand which induced false reading in the displacement sensor. The silicone glue used in the actuator fabrication withstands temperatures up to 700°F. Hence, it was not considered a source of error.
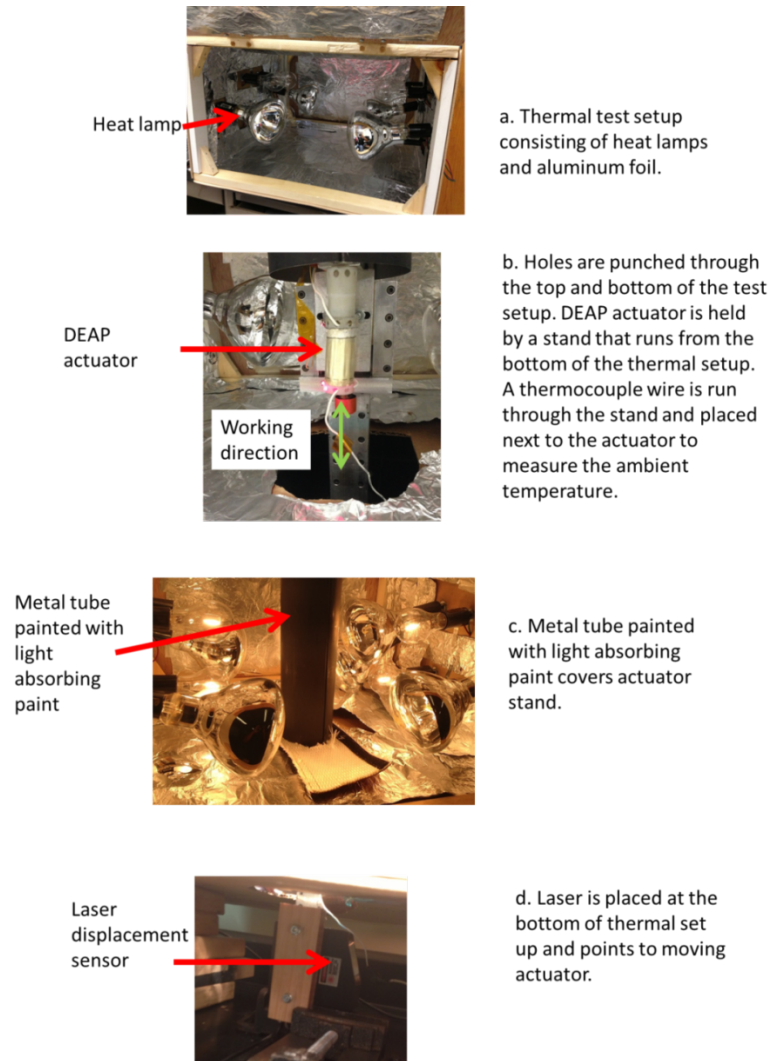
Figure A.1 Photo of thermal test bench. a) General view of setup showing the heat lamps and aluminum foil. b) Actuator mounted on test stand inside thermal setup. c) Metal tube painted with light absorbing paint covering actuator d) View of laser displacement sensor placed at the bottom of the test bench.

Figure A.2 shows the experimental results of the thermal tests. As shown, the amount of stroke produced decreases with increasing temperature at voltages higher than

750V. The decrease in performance is more significant at voltages between 1.25kV and 2kV. However at higher voltages the effects of temperature are small.

While the full temperature range (-40°F and 212°F) was not tested, modifications to the actuator test stand can be done to insure thermal expansion is not a factor. This means building a new actuator test stand with temperature insulating materials is needed.
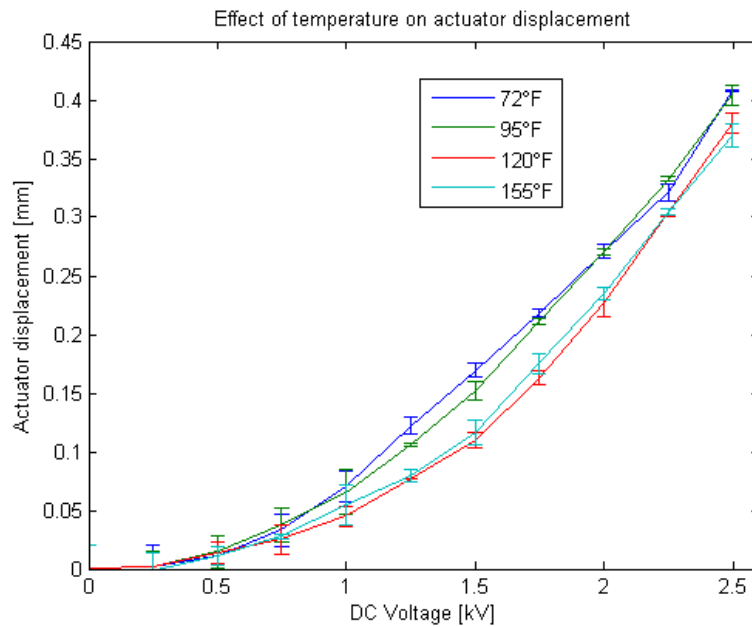
Figure A.2 DEAP actuator output displacement as a function of voltage at different ambient temperatures.

Appendix B

Circuit Model

A circuit model of the spring roll actuator is presented here. The modeling and simulation are done using the LTspice software. The actuator's frequency and transient response of the simulations are compared to experimental results.

B.1 Actuator Modeling

The model is a combination of two sub-models describing the mechanical and electrical parts of the actuator system. These two sub-models are coupled by Pelrine's equation described in chapter 1. The following assumptions are made for this model:

- Linear elastic material behavior.
- Capacitance of material does not change with voltage due to the small induced strains

B.1.1 Mechanical Model

The behavior of the DEAP material is modeled by a combination of a linear elastic spring, a dashpot and a mass. An additional linear elastic spring is used to model the pre-strain element (see figure B.1). As shown in B.1, the stiffness of the DEAP material is represented by K_{DEAP}, the damping by C_{DEAP} and the moving mass of the actuator by m. The spring's constant of the bias spring is represented by K_{bias} and the electrostatic forces by F
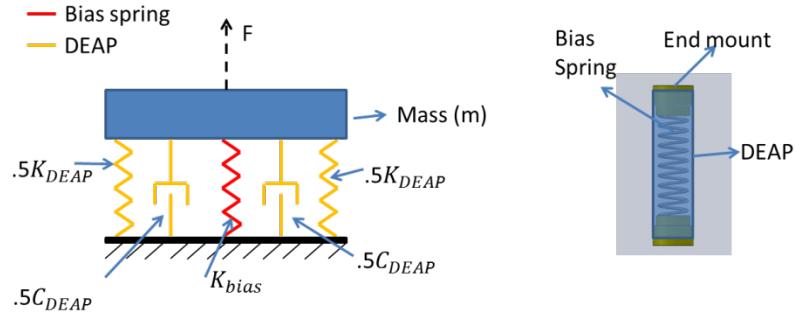
Figure B.1: Mechanical model of spring roll actuator (left), schematic of spring roll actuator (right)

B.1.2 Electrical Model

The DEAP material is essentially a compliant capacitor with capacitance C and resistance R as shown in figure B.2. The capacitance of the material is assumed constant because of the low values of strain achieved at max voltage. The activation voltage is represented by V_a.
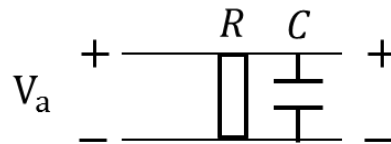
Figure B.2: Electrical representation of DEAP material. R and C represent the resistance and capacitance of the material. V_a represents the activation voltage across the material.

B.1.3 Electromechanical Model

The electromechanical coupling between the electrical input and the mechanical shape change is given by Pelrine's equation (see equation B.1 and figure B.3).

$$P = \varepsilon_o \varepsilon_r \left(\frac{V}{t}\right)^2 \qquad\qquad \text{B.1}$$
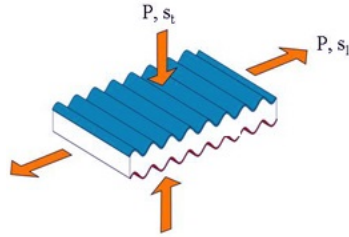
Figure B.3: Schematic of unidirectional DEAP material under the electrostatic pressure P. The strain in the thickness direction is given by s_t and in the longitudinal direction by s_l[9].

The permittivity of vacuum, the relative permittivity of the DEAP material, and the distance between the electrodes are given by e_r, e_o and t. The electrostatic pressure and the applied voltage are represented by P and V. The amplitude of the corrugation is much smaller than the thickness of the elastomer dielectric hence it is considered negligible. Figure B.4 shows a schematic representation of the electromechanical model. The input voltage V_a generates an electrostatic pressure P. This electrostatic pressure is input to the mechanical domain resulting in a displacement of the moving mass (m).
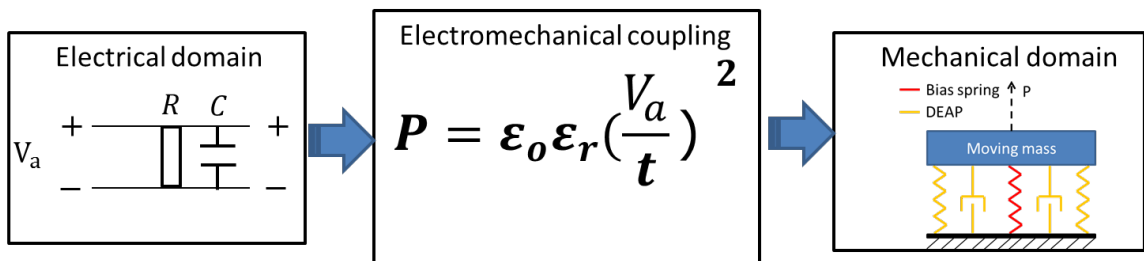
Figure B.4: Schematic of electromechanical model. Electrical domain of the actuator (left), electromechanical coupling equation (middle), mechanical domain of actuator (right)

In order to analyze the model as a circuit, the electrical equivalent of the mechanical domain is needed. Looking at the basic electrical elements and their

81

respective mathematical representations, an equivalency to the basic mechanical elements can be drawn. For example, the voltage u across an inductor is given by equation B.2 where L is the inductance value and i the current through the inductor.

$$u = L * \frac{di}{dt} \qquad \text{B.2}$$

In a similar way, the rate of change of the force in a spring can be described by its velocity v and compliance n (see equation B.3).

$$v = n\frac{dF}{dt} \qquad \text{B.3}$$

By looking at equations B.2 and B.3, the equivalency between the compliance of the spring and the inductance of the inductor is demonstrated. It can be also seen that the current is equivalent to the mechanical force and the voltage to the velocity. A complete list of analogies is shown in table B.1.

Table B.1 List of analogies between electrical and mechanical domains

Electrical	Symbol	Mechanical
Voltage	$u <-> v$	Velocity
Current	$i <-> F$	Force
Inductance	$L <-> n$	Compliance
Capacity	$C <-> m$	Mass
Resistance	$R <-> h$	Friction admittance
Conductance	$G <-> r = 1/h$	Friction impedance

Symbolical representation of the electromechanical analogies used in this model is shown in figure B.5.
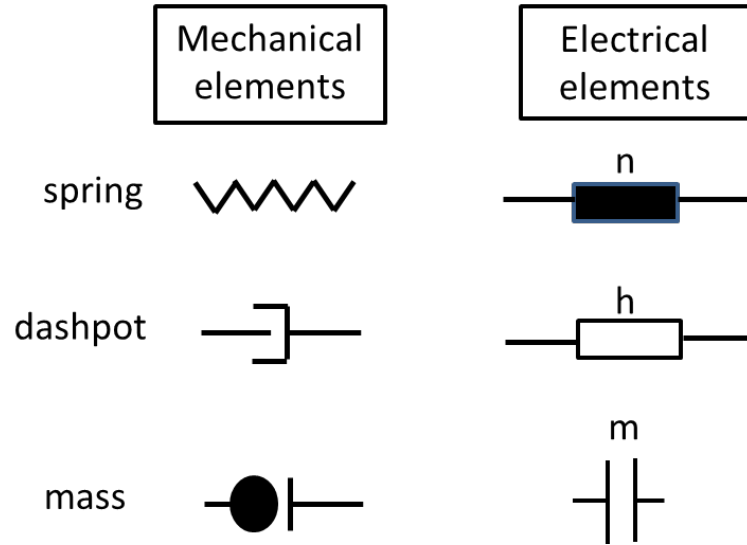
Figure B.5 Graphical representation of mechanical elements (left) and electrical elements (right)

Therefore, the corresponding electrical circuit of the model is shown in figure B.6 below.
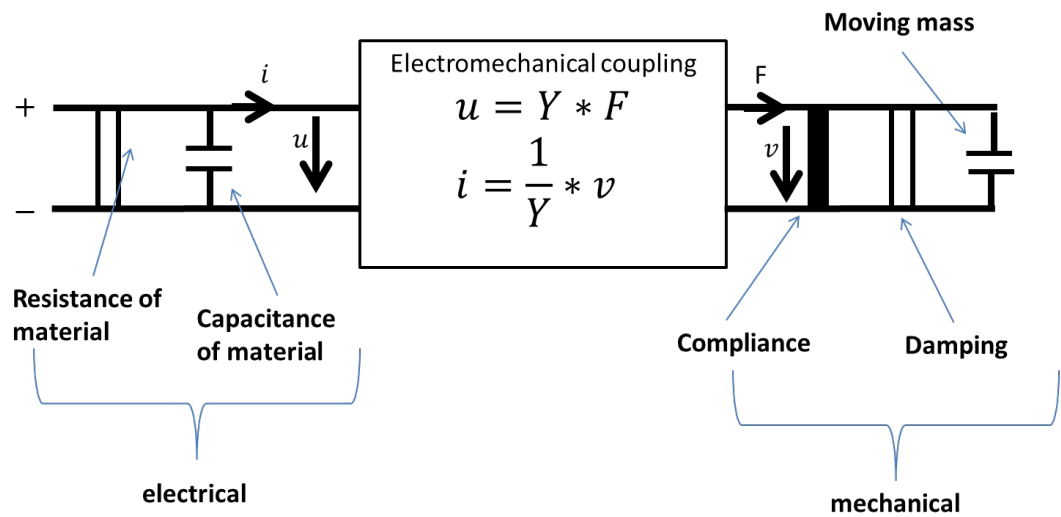
Figure B.6 Circuit representation of electromechanical model with electrical domain on the left and mechanical domain on the right.

An additional step is needed in order to insert this circuit model into the LTspice software. The electrical domain is transferred to the mechanical domain via the

electromechanical coupling equations. As seen in transducer box in figure B.6, the parameter Y relates the across quantity, u (voltage), in the electrical domain to the through quantity F (force) in the mechanical domain. The same is for the current and velocity (through and across quantities). This transduction box is known as a gyrator and it relates quantities an across quantity to a through quantity and vice versa. When the electrical elements are transferred to the mechanical domain their quantities are normalized by the factor Y and appear in series due to the gyrator.

The parameter Y is found through a linearization procedure found in the literature [32] and its derivation will not be shown. The parameter Y is given by equation B.4 where A is the actuator effective area given by $(w_a * t * 2)$ and u_o is the magnitude of the applied voltage. The final circuit model is shown in figure B.7. The force source is given by equation B.1 divided by the actuator cross sectional area A.

$$Y = \frac{t}{e_o e_r A u_o} \qquad \text{B.4}$$
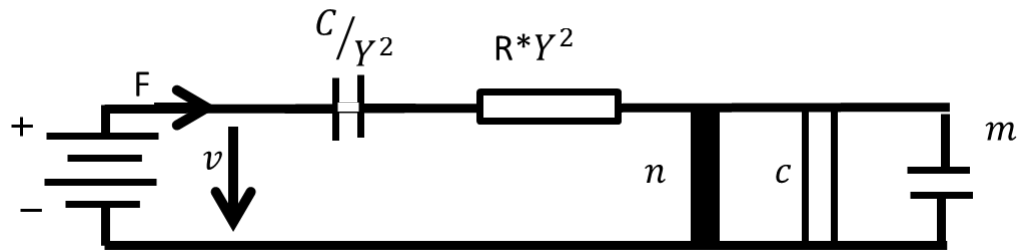
B.7 Final circuit representation of spring roll actuator in the mechanical domain.

B.1.4 Parameter Identification

The electrical and mechanical parameters where found experimentally. The stiffness of the DEAP film was found based on tensile load tests performed in chapter 4

and the damping parameter based on the settling time of step response tests. The inertial parameter M is given by equation B.2.

$$m = m_{DEAP} + m_{mount} + m_{bias} \qquad \text{B.2}$$

In the equation above, m_{DEAP} is the mass of the active and upper passive parts of the film. They are calculated from the known volume and mass density of the material. The lower passive region is not moving hence is not taken into account. The mass of the moving end mount is given by m_{mount} and the mass of the bias spring is given by m_{bias}. The capacitance and resistance of the actuator are measured with a conventional multimeter. Table B.2 lists all the parameters in the model. The corresponding circuit elements values are shown in table B.3.

Table B.2: List of actuator parameters for circuit model

Parameter	Value
K_{DEAP}	280 N/m
K_{bias}	245 N/m
h_{DEAP}	35.5 N m/s
m_{DEAP}	.5 g
m_{mount}	1.2 g
m_{bias}	.06 g
C	5.2pF
R	14GΩ

Table B.3 List of electromechanical parameters for circuit model

Parameter	Value
n	280 N/m
m	1.8 g
h	35.5 N m/s
C	5.2 pF
R	14GΩ
Y(2500V)	$6.7 * 10^7$

B.1.5 Simulation Results

The electromechanical model is implemented on the LTspice software as shown in figure B.8. The displacement frequency and transient response is compared to the spring roll experimental results.
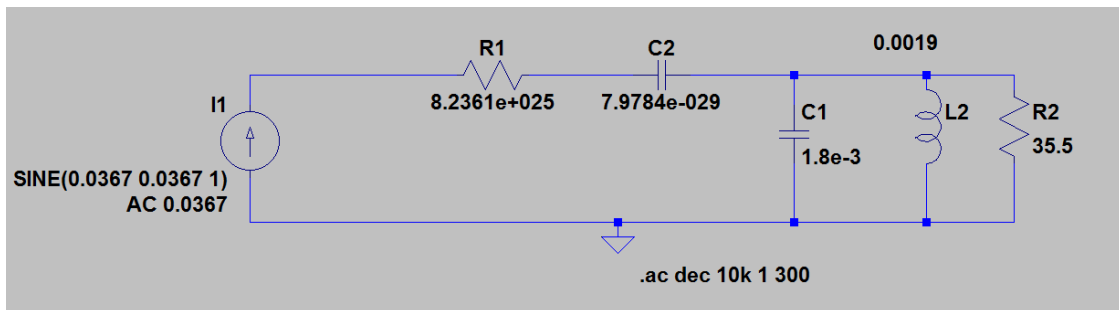
Figure B.8 Snapshot of circuit model on the LTspice software. Values in this case are based on a sine force input at 1500V p-p.

As shown in figure B.9, the model captures the furthest peak seen in the experimental results. This peak is attributed to the system's resonance frequency. The experimental and model's transient response to a sine input (2500V p-p) is shown in

figure B.10. The magnitude of the model's displacement response is close to the experimental results. This close agreement between the model and experimental results suggests the actuator follows the behavior of a damped harmonic oscillator. Although this model is simple, it provides a good starting point to the exploration of the dynamics of a DEAP actuator.
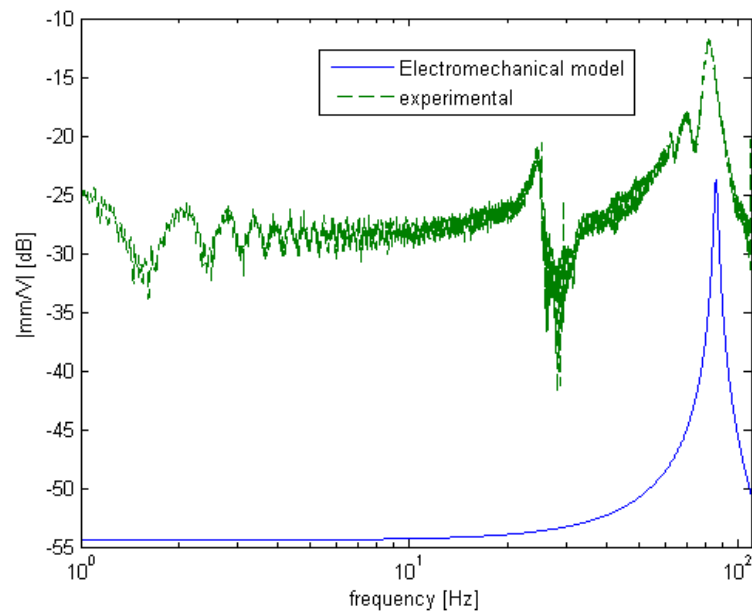
Figure B.9 Displacement frequency response of spring roll actuator (green) and electromechanical (model). Input voltage frequency sweep of 1500 p-p 1Hz to 110Hz.
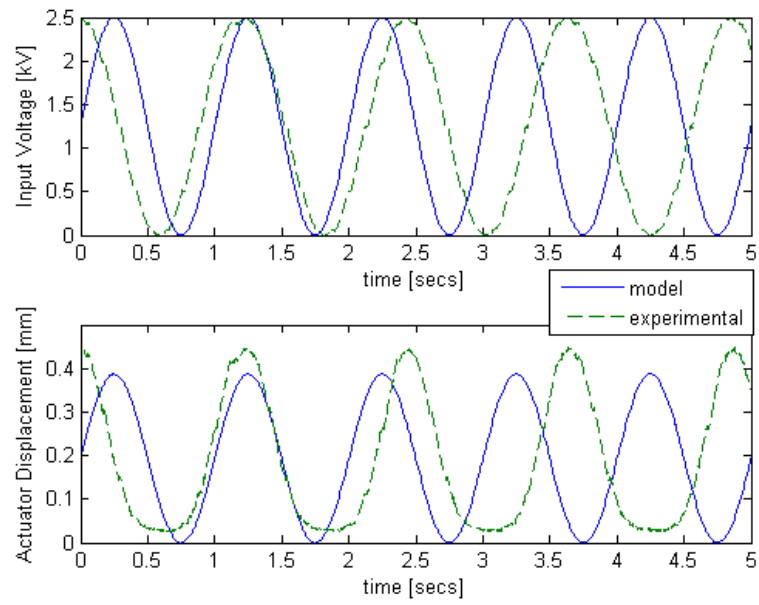
Figure B.10 Transient response of model (blue) and actuator (green) to a 1Hz 2500V p-p sine input.

Appendix C

Carbon Fiber Tensile Load Test

A specimen of a single carbon fiber composite laminate was tested in a MTS machine. The specimen was 6 inches long, .15 in wide and .006 thick. Thi tensile test provided the value of the Young's modulus of the material. Figure C.1 shows the experimental results.
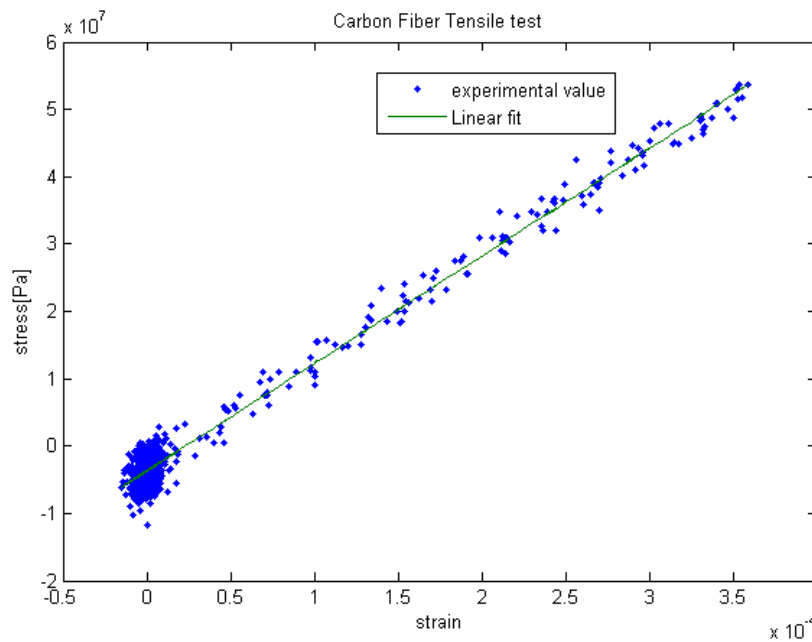
Figure C.1 Stress vs. strain behavior of carbon fiber composite laminate and its corresponding linear fit.

The Young's Modulus of the material was found to be $1.59*10^{11}$ Pascals or 160GPa. This value is used in chapter 5 to size the carbon fiber beams of the constant force mechanism.

Bibliography

[1] Carpi, Fererico, Danilo De Rossi, Roy Kornbluh, Ronald Pelrine, and Peter Sommer-Larsen, eds. *Dielectric Elastomers as Electromechanical Transducers Fundamentals, Materials, Devices, Models and Applications of an Emerging Electroactive Polymer Technology*. Oxford: Elsevier, 2008.

[2] C. Huang, Q. Zhang, "Electroactive polymer (EAP)-based deformable micromirrors and light-valve technology for MOEMS display and imaging systems", in *Proc. of SPIE 5389*, Smart Structures and Materials 2004: Smart Electronics, MEMS, BioMEMS, and Nanotechnology, 274 (July 29, 2004)

[3] Y. Y. Jhong, C. M. Huang, C. C. Hsieh, and C. C. Fu, "Improvement of viscoelastic effects of dielectric elastomer actuator and its application for valve devices", in *Proc. of SPIE EAPAD*, 2007, pp. 1-9.

[4] Q. Pei, M. Rosenthal, R. Pelrine, S. Stanford, and et.al., "Multifunctional electroelastomer roll actuators and their application for biomeimetic walking robots", in *Proc. of Smart Structures and Materials*, vol. 5051, 2003, pp.281-290.

[5] J. S. Plante, "Dielectric elastomer actuators for binary robotics and mechatronics", PhD thesis, Massachusetts Institute of Technology, Cambridge, MA, 2006.

[6] N. Goulbourne, M. Frecker, and E. Mockensturm, "Electro-Elastic Modeling of a Dielectric Elastomer Diaphragm for a Prosthetic Blood Pump", in *Proc. of SPIE EAPAD*, 2004, pp. 122-133.

[7] Lochmatter, P., and G. Kovacs. "Design and Characterization of an Active Hinge Segment Based on Soft Dielectric EAPs", *Sensors and Actuators A: Physical*141.2 (2008): 577-87. Print.

[8] Heydt, R., Kornbluh, R., Eckerle, J. and Pelrine, R. (2006). "Sound radiation properties of electroactive polymer loudspeakers", *Proceeding of the SPIE Conference on Smart Structures and Materials*, San Diego, California, USA.

[9] *http://www.polypower.com/*

[10] Bar-Cohen Y., "Electroactive Polymer (EAP) Actuators as Artificial Muscles - Reality, Potential and Challenges", 2nd Edition, ISBN 0-8194-5297-1, SPIE Press, Vol. PM136, (March 2004), pp. 1-765.

[11] R. A. Anderson, "Mechanical stress in a dielectric solid from a uniform electric field", *Physical Review B (Condensed Matter),* vol. 33, pp. 1302-7, 1986.

[12] M. Zhenyi, J. I. Scheinbeim, J. W. Lee, and B. A. Newman, "High field electrostrictive response of polymers", *Journal of Polymer Science, Part B: Polymer Physics,* vol. 32, pp. 2721-2731, 1994.

[13] R. Pelrine, R. Kornbluh, and J. Joseph, "Electrostriction of Polymer Dielectrics with Compliant Electrodes as a Means of Actuation", *Sensors and Actuators A: Physical,* vol. 64, pp. 77-85, 1998.

[14] R. Pelrine, R. Kornbluh, Q. Pei, and J. Joseph, "High-speed electrically actuated elastomers with strain greater than 100%", *Science,* vol. 287, pp. 836-839, 2000.

[15] R. Pelrine, R. Kornbluh, Q. Pei, S. Stanford, S. Oh, J. Eckerle, R. Full, M. Rosentha, and K. Meijer, "Dielectric elastomer artificial muscle actuators: Toward biomimetic motion", *Proceedings of SPIE*, vol. 4695, pp. 126-137, 2002.

[16] F. Carpi, A. Chiarelli, and A. Mazzoldi, "Electromechanical Characterization of Dielectric Elastomer Planar Actuators: Comparative Evaluation of Different Electrode materials and Different Counterloads," *Sensors and Actuators A: Physical,* vol. 107, pp. 85-95, 2003.

[17] F. Carpi, P. Chiarelli, A. Mazzoldi, and D. DeRossi, "Electromechanical characterization of dielectric elastomer planar actuators: comparative evaluation of different electrode materials and different counterloads," *Sensors and Actuators,* pp. 85-95, 2003.

[18] F. Carpi, A. Migliore, G. Serra, and D. De Rossi, "Helical dielectric elastomer actuators," *Smart Materials and Structures*, vol. 14, pp. 1210-1216, 2005.

[19] F. Carpi, C. Salaris, and D. De Rossi, "Folded dielectric elastomer actuators," *Smart Materials and Structures,* vol. 16, pp. 300-305, 2007.

[20] F. Carpi and D. de Rossi, "Dielectric Elastomer Cylindrical Actuators: Electromechanical Modelling and Experimental Evaluation," *Journal of Materials Science and Engineering C,* vol. 24, pp. 555-562, 2004.

[21] Carpi, Federico. "Chapter 4.4 Silicones and Acrylics." Dielectric Elastomers as Electromechanical Transducers: Fundamentals, Materials, Devices, Models and Applications of an Emerging Electroactive Polymer Technology. Oxford, UK: Elsevier, 2008.

[22] Kofod, G., Kornbluh, R., Pelrine, R. and Sommer-Larsen, P. (2001). Actuation response of polyacrylate die-lectric elastomers. In *Smart Structures and Materials: Electroactive Polymer Actuators and Devices (EAPAD)*, Ed. Bar-Cohen, Y., Proc. SPIE, 4329, 141–147.

[23] Kornbluh, R., Pelrine, R., Pei, Q., Oh, S. and Joseph. J. (2000). Ultrahigh strain response of field-actuated elastomeric polymers. In *Smart Structures and Materials 2000: Electroactive Polymer Actuators and Devices (EAPAD)*, Ed. Bar-Cohen, Y., Proc. SPIE, 3987, June, 51–64.

[23] R.E. Pelrine, R.D. Kornbluh, J.P. Joseph, Electrostriction of polymer dielectrics with compliant electrodes as a means of actuation, *Sens. Actuators*, A 64 (1998) 77-85

[24] G. Kofod, P. Sommer-Larsen, Silicone dielectric elastomer actuators: Finite-elasticity model of actuation, *Sens. Actuators*, A 122 (2005), 273-283

[25] R.E. Pelrine, R.D. Kornbluh, J.P. Joseph, Electrostriction of polymer dielectrics with compliant electrodes as a means of actuation, *Sens. Actuators*, A 64 (1998) 77-85

[26] Luan, Yunguang, Huaming Wang, and Yinlong Zhu. "Design and Implementation of Cone Dielectric Elastomer Actuator with Double-Slider Mechanism." *Journal of Bionic Engineering* 7 (2010): S212-217. Print.

[27] R. Zhang, P. Lochmatter, A. Kunz, et al., "Spring roll dielectric elastomer actuators for a portable force feedback glove", In. *Proc. of SPIE Smart Struct. and Mat.: Electroactive Polymer Actuators and Devices (EAPAD)*, volume 6168.

[28] S. Arora, T. Ghosh, and J. Muth, "Dielectric elastomer based prototype fiber actuators," *Sensors and Actuator A*, vol. 136, pp. 321-328, 2007.

[29] Carpi, Federico. "Chapter 8.2 Basic Configurations." *Dielectric Elastomers as Electromechanical Transducers: Fundamentals, Materials, Devices, Models and Applications of an Emerging Electroactive Polymer Technology*. Oxford, UK: Elsevier, 2008.

[30] F. Carpi, D. De Rossi, "Dielectric elastomer cylindrical actuators: electromechanical modeling and experimental evaluation", *Materials Science and Engineering*, C 24, pages 555-562, 2004

[31] Tryson, M.J., Kiil, H.E. and Benslimane, M. Y., "Powerful tubular core free dielectric electro active polymer (DEAP) push actuator", *Proceedings of SPIE* 7287, 72871F-1 (2009).